ABSTRACT

Title of Dissertation: DETERMINING THE NEUTRINO LIFETIME FROM COSMOLOGY

Abhish Dev,
Doctor of Philosophy, 2021

Dissertation Directed by: Professor Zackaria Chacko
Department of Physics

Neutrinos are the most mysterious particles in the standard model. Many of their fundamental properties such as their masses, lifetimes, and nature (Dirac or Majorana) are yet to be pinned down by experiments. Currently, the strongest bound on neutrino masses comes from cosmology. This bound is obtained by scrutinizing the gravitational effect of the cosmic neutrinos on the evolution of structure in our universe. However, this bound assumes that the neutrinos from the Big Bang have survived until the present day. In this dissertation, the unstable neutrino scenario is studied in light of current and near-future cosmological experiments. We show that the current cosmological bound on the neutrino masses can be relaxed significantly in an unstable neutrino scenario. We further show that near-future experiments offer the possibility of independently measuring both the masses of the neutrinos and their lifetimes.

We consider an elusive scenario in which the cosmic neutrinos decay into invisible radiation after becoming non-relativistic. The Boltzmann equations that govern the cosmological evolution of density perturbations in the case of unstable neutrinos are derived and solved

numerically to determine the effects on the matter power spectrum and lensing of the cosmic microwave background (CMB). A Markov-Chain Monte-Carlo (MCMC) analysis is done on the current cosmological data and mock future data to obtain its sensitivity to the neutrino masses and lifetimes. We show that the effect of the neutrino masses on large scale structure is dampened by the decay of neutrinos, which leads to a parameter degeneracy between the neutrino masses and lifetimes inferred from the cosmological data. This degeneracy allows for a significant relaxation of the current cosmological upper bound on the sum of neutrino masses from about $0.2\ eV$ in the stable neutrino case to $0.9\ eV$ in the unstable neutrino scenario. This window is important for terrestrial experiments such as KATRIN which are seeking to independently measure the neutrino masses in the laboratory. We further show that near-future large scale structure measurements from the Euclid satellite, when combined with cosmic microwave background data from Planck, may allow an independent determination of both the lifetimes of the neutrinos and the sum of their masses. These parameters can be independently determined because the Euclid data will cover a range of redshifts, allowing the growth of structure over time to be tracked. If neutrinos are stable on the timescale of the age of the universe, we show that these observations can improve the lower limit on the lifetimes of the neutrinos by seven orders of magnitude, from $O(10)$ years to 2×10^8 years$(95\% C.L.)$, without significantly affecting the measurement of the neutrino masses. On the other hand, if neutrinos decay after becoming non-relativistic but on timescales less than $O(100)$ million years, these observations may allow for, not just the first measurement of the sum of neutrino masses, but also the determination of the neutrino lifetime from cosmology.

DETERMINING THE NEUTRINO LIFETIME FROM COSMOLOGY

by

Abhish Dev

Dissertation submitted to the Faculty of the Graduate School of the
University of Maryland, College Park in partial fulfillment
of the requirements for the degree of
Doctor of Philosophy
2021

Advisory Committee:
Professor Zackaria Chacko, Chair/Advisor
Professor Alberto Belloni
Professor Anson Hook
Professor Rabindra Mohapatra
Professor Massimo Ricotti
Professor Raman Sundrum

Dedication

To my parents - Valsa Dev and Kutty Sahadevan, and my aunt - Annamma Johnson Manappallil, for their love, encouragement, and support in every step of my life

Table of Contents

List of Tables

List of Figures

List of Abbreviations

BAO	Baryon Acoustic Oscillation
BBN	Big Bang Nucleosynethesis
BOSS	Baryon Oscillation Spectroscopic Survey
BSM	Beyond the Standard Model
CDM	Cold Dark Matter
CLASS	Cosmic Linear Anisotropy Solving System
CMASS	Constant Stellar Mass
CMB	Cosmic Microwave Background
CMB-S4	CMB-Stage 4
CνB	Cosmic Neutrino Background
EXO	Enriched Xenon Observatory
GUT	Grand Unified Theory
KATRIN	KArlsruhe TRItium Neutrino
KLZ	KamLand-Zen
KiDS	Kilo-Degree Survey
LSS	Large Scale Structure
MCMC	Markov Chain Monte Carlo
PNGB	Pseudo-Nambu–Goldstone Bosons
QFT	Quantum Field Theory
SDSS	Sloan Digital Sky Survey
SM	Standard Model
SNe	Supernovae
SSB	Spontanoeus Symmetry Breaking
VEV	Vacuum Expectation Value

Chapter 1: Introduction

Neutrinos are the most elusive particles in the SM. Their interactions with the rest of the SM are only mediated through the weak interactions and gravity, which makes it challenging to probe them in experiments. Their existence was first proposed by Wolfang Pauli in 1930 to explain the observed continuous energy spectrum of the emitted beta particle (electron or positron) in the nuclear beta decay process. It was then believed that in the beta decay process, a neutron (proton) in a radioactive nucleus is converted into a proton (neutron) along with the emission of an electron (positron). In this picture, the laws of conservation of energy and momentum require that the emitted electron be monochromatic. However, it was observed that the electron from the beta decay has a continuous energy spectrum. To explain this, Pauli proposed that a new electrically neutral particle that is either massless or very light is also emitted in the final state. Since this new particle had escaped detection, it must also be very feebly interacting with the matter. This three-body nature of the beta decay now admits enough additional degrees of freedom in the form of neutrino kinematic parameters to allow the electron to have a continuous range of energy while satisfying both energy and momentum conservation. And thus, the neutrino was born.

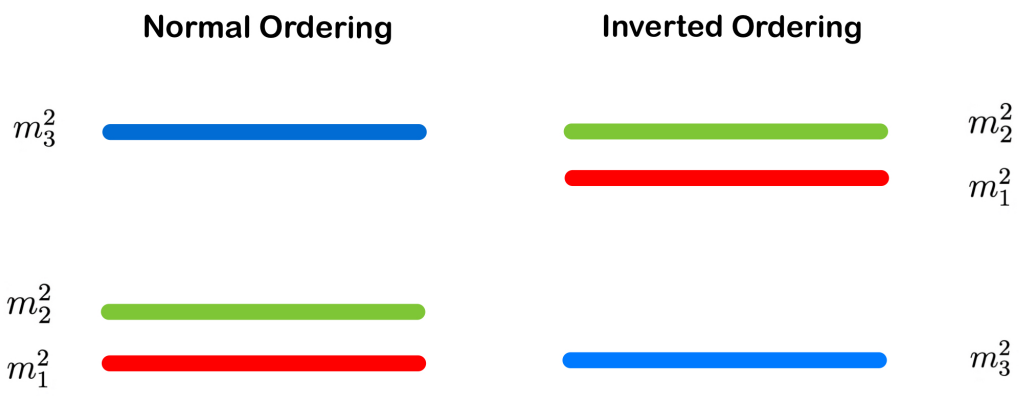

Figure 1.1: Normal and inverted ordering of neutrino masses

Since the 1930s, the number of observed elementary particles has greatly increased leading to the current Sm of particle physics. SM of particle physics is a gauge theory based on the symmetry $G_{SM} \equiv SU(3)_C \times SU(2)_L \times U(1)_Y$. Here, $SU(3)_C$ corresponds to the strong interactions while $SU(2)_L \times U(1)_Y$ together give rise to weak and electromagnetic interactions. At low energies, $SU(2)_L \times U(1)_Y$ is spontaneously broken via " Higgs Mechanism" to its residual subgroup $U(1)_Q$ which constitutes our familiar electromagnetic and color gauge symmetries. This spontaneous symmetry breaking (SSB) is achieved with a complex spin-0 Higgs field that transforms as a doublet of $SU(2)_L$. After the SSB, three out of four components of the complex doublet become part of the gauge bosons, thus leaving behind a single neutral spin-0 particle called the Higgs boson. The spin-1 gauge bosons, both massive and massless, constitute the force carriers in this model. The massless gauge bosons corresponding to the exact electromagnetism $U(1)_Q$ and color symmetry $SU(3)_C$ are the photon and the gluons that mediate the electromagnetic force and the strong nuclear forces respectively. The gauge bosons corresponding to the

spontaneously broken symmetry acquire a mass by "eating the Goldstone bosons" which become the longitudinal polarization of these gauge bosons. These are the heavy gauge bosons $(W^{\pm}, Z)$ that mediate the weak nuclear force.

In addition to these bosonic fields, the SM contains many spin-1/2 fermionic fields which constitute the matter sector of the theory. These fermions transform under the SM gauge group. These fermions (Ψ) are chiral in the sense that their left-handed and right-handed components (Ψ_L and Ψ_R) transform differently under the SM gauge symmetry G_{SM}. These chiral fermions come in three generations with each generation having both a quark branch consisting of an up-type quark and a down-type quark and a leptonic branch consisting of a charged lepton and a neutrino. In particular, the charged lepton $(e,\ \mu,\ \tau)$ along with their respective neutrino $(\nu_e,\ \nu_\mu,\ \nu_\tau)$ form the leptonic branches of the first, second, and third generations (families) respectively. Each of the quarks also come in three colors which leads to strong interaction among the quarks. The left-handed up- and down-type quarks together transform as a fundamental doublet of the $SU(2)_L$ and the right-handed quarks are $SU(2)_L$ singlets. Similarly, the charged lepton with its corresponding neutrino also transform as an $SU(2)_L$ doublet. The right-handed charged lepton transforms as an $SU(2)_L$ singlet as in the case of right-handed quarks. However, unlike the quarks and the charged leptons, the SM does not contain a field corresponding to the right-handed neutrino. As we shall see, this implies that in the SM, the neutrinos are necessarily massless.

The feeble interaction of neutrinos posed challenges in the experimental detection of neutrinos. The neutrino was directly detected for the first time in 1956 by Clyde Cowan, Frederick Reines, Francis B. Harrison, Herald W. Kruse, and Austin D. McGuire

in the process $\bar{\nu}_e + p^+ \rightarrow n^0 + e^+$. In 1962, Leon M. Lederman, Melvin Schwartz and Jack Steinberger detected the muon neutrino that was already hypothesised as the neutral partner of muon. The direct detection of tau neutrinos had to wait until the 2000s when it was observed by DONUT collaboration at Fermilab.

Neutrino oscillation experiments have established that the neutrinos have masses. The explanation for neutrino masses requires physics Beyond the Standard Model (BSM). In a relativistic quantum field theory (QFT), there are two possible Lorentz-invariant bilinears for fermions that can be constructed. This is because the left- and right-handed components of the Dirac spinor transform as independent, irreducible representations of the Poincare group. This allows for two kinds of mass terms for fermions, namely Dirac and Majorana mass :

$$\begin{aligned} \mathcal{L} &\supset -m\overline{\Psi}_R\Psi_L + h.c. = -m\overline{\Psi}\Psi, \text{ where } \Psi = \Psi_L,\ \Psi_R \text{ (Dirac) and} \qquad (1.1) \\ \mathcal{L} &\supset -m\frac{1}{2}\Psi_L^T C^{-1}\Psi_L + h.c. = -\frac{1}{2}m\overline{\Psi}\Psi, \text{ where } \Psi = \Psi_L,\ (\Psi_L)^c \text{ (Majorana).} \end{aligned}$$

Here, C refers to the charge conjugation matrix. Physically, this means that the fermion and anti-fermion are distinct particles if the fermions have a Dirac mass term, while the fermions are their own anti-particles if they have a Majorana mass term. The form of Majorana mass term in Eq. (1.1) can also be seen to violate any $U(1)$ global charge that these fermions might have. Since all the SM fermions except neutrinos are electrically charged, this forbids them from having a Majorana mass term.

If the SM neutrinos are Dirac fermions, this would necessitate the addition of right-handed neutrinos to the theory. However, their direct detection could pose a challenge.

In the electroweak theory, parity is violated and only the left-handed fermions experience the weak interactions. Since neutrinos only experience weak interactions, the interactions of right-handed neutrinos with experimentalists are non-existent for massless neutrinos and doubly suppressed by both the weak interaction coupling and the small neutrino mass in the case of massive neutrinos.

To understand this better, let us look at the origin of fermion masses in the standard model (SM). In the SM, the fermion masses are generated via the Higgs mechanism. The left-handed fermions come in an $SU(2)_L$ doublet whereas the right-handed neutrinos are $SU(2)_L$ singlets. Because of this chiral nature, it is not possible to write a vector-like mass term for these SM fermions. The presence of the additional scalar Higgs doublet H allows us to write a $SU(2)_L$-invariant Yukawa interaction term for the leptons as

$$-\mathcal{L}_{Yukawa,lep} = Y^l_{ij}\bar{L}_{Li}Hl_{Rj} + h.c. \quad \text{or} \quad Y^l_{ij}\bar{L}_{Li}\tilde{H}l_{Rj} + h.c. \tag{1.2}$$

where L_{Li} is the left-handed lepton doublet of the i^{th} generation and l_{Rj} is the right-handed $SU(2)_L$ singlet of the j^{th} generation and $\tilde{H} \equiv i\sigma_2 H^*$. After the electroweak symmetry breaking, the Higgs field takes a vacuum expectation value (VEV) which leads to the mass term for charged lepton mass matrix

$$M^l_{ij} = Y^l_{ij}\frac{v}{\sqrt{2}}, \tag{1.3}$$

where $\langle H \rangle \equiv v$ is the VEV of the SM Higgs. In the SM, the right handed neutrinos are taken to be absent which also explained the vanishing neutrino masses. However,

neutrinos are not considered to be massless anymore. This is due to the discovery of flavor oscillations in the neutrino sector.

The standard picture of massless neutrinos faced its first major challenge in the 1960s with the Homestake experiment conducted by Raymond Davis Jr. and John N. Bachall, which was designed to detect and count the number of electron neutrinos emitted from the nuclear fusion process in the sun. In this experiment, a 100, 000 gallon tank of dry cleaning fluid was placed underground deep enough to shield it from cosmic rays. The electron neutrinos from the sun can penetrate the earth. Some neutrinos are captured by the chlorine atoms in the fluid, which in this process gets converted to argon atoms. These argon atoms can then be extracted and counted. This experiment consistently gave a number that was one-third of the theoretical expectations from the standard solar model. This deficit can be explained by the phenomenon of neutrino flavor oscillations which can happen if a) neutrinos have masses, b) neutrino mass eigenstates are mixed in weak interactions, and c) lepton flavor number is not conserved. This is a purely quantum effect where the neutrinos are emitted and detected as flavor eigenstates but during the journey from the source to the detector, they are in a quantum superposition of various mass eigenstates. The phenomenon of particle oscillations had already been observed in the case of neutral kaons in particle.

The theory of mass-induced oscillations among neutrinos can be understood as follows. The flavor of a neutrino is determined by the charged lepton that it interacts with via weak interactions. Below the electroweak scale, the mass term for neutrinos (

whether Dirac or Majorana) can couple neutrinos of different flavors as

$$\begin{aligned}\mathcal{L} &\supset \frac{g}{\sqrt{2}}\sum_{\alpha=e,\mu,\tau}\bar{l}_\alpha\gamma^\mu P_L\nu_\alpha W_\mu^- + \sum_{\alpha,\beta=e,\mu,\tau}\bar{\nu}_\alpha M_{D\alpha\beta}\nu_\beta + h.c. \text{ (Dirac) or} \\ &\supset \frac{g}{\sqrt{2}}\sum_{\alpha=e,\mu,\tau}\bar{l}_\alpha\gamma^\mu P_L\nu_\alpha W_\mu^- + \frac{1}{2}\sum_{\alpha,\beta=e,\mu,\tau}\bar{\nu}_\alpha M_{M\alpha\beta}\nu_\beta + h.c. \text{ (Majorana),}\end{aligned} \tag{1.4}$$

where the Dirac mass matrix M_D is , in general, a complex 3×3 matrix while the Majorana mass matrix M_M is a complex symmetric 3×3 matrix. This means that a neutrino of definite flavor does not have a definite mass but is, instead, a superposition of various mass eigenstates. We can go to the mass basis ν_i $(i = 1, 2, 3)$ which is related to the flavor basis $\nu_\alpha(\alpha = e, \mu, \tau)$ via a unitary rotation,

$$\nu_\alpha = \sum_i U_{\alpha i}\nu_i \text{ where } \alpha = e, \mu, \tau \text{ and } i = 1, 2, 3. \tag{1.5}$$

In the mass basis, the Lagrangian becomes

$$\begin{aligned}\mathcal{L} &\supset \frac{g}{\sqrt{2}}\sum_{\alpha=e,\mu,\tau}\sum_{i=1,2,3}\bar{l}_\alpha\gamma^\mu P_L U_{\alpha i}\nu_i W_\mu^- + \sum_{i=1,2,3} m_{\nu i}\bar{\nu}_i\nu_i + h.c. \text{ (Dirac) or} \\ &\supset \frac{g}{\sqrt{2}}\sum_{\alpha=e,\mu,\tau}\sum_{i=1,2,3}\bar{l}_\alpha\gamma^\mu P_L U_{\alpha i}\nu_i W_\mu^- + \frac{1}{2}\sum_{i=1,2,3} m_{\nu i}\bar{\nu}_i\nu_i + h.c. \text{ (Majorana).}\end{aligned} \tag{1.6}$$

Now, we can understand the oscillation phenomena in a simple quantum mechanical framework. Consider a neutrino eigenstate ν_i of definite mass m_i. After travelling a distance L in time t ($t \sim L/c$ for relativistic neutrinos), the wave function evolves via

the Hamiltonian as

$$|\nu_i(t)\rangle = e^{-iE_i t}|\nu_i(0)\rangle \text{ with } E_i = \sqrt{p^2 + m_i^2}. \tag{1.7}$$

If we instead consider a neutrino of definite flavor α that is produced at source (for example, neutrinos are produced in the sun with a pure electron flavor), it is a superposition of various mass eigenstates each of which evolves independently via Eq. (1.7). After evolving for some time t, the wave packet is not a pure flavor eigenstate anymore but is instead a combination of different flavor eigenstates. Now, the probability for a neutrino of energy E produced of some flavor α to get converted to flavor β after travelling L distance is given as

$$\begin{aligned} P_{\alpha\beta} &= |\langle \nu_\beta \mid \nu_\alpha(t)\rangle|^2 = \left| \sum_{i=1}^{3}\sum_{j=1}^{3} U^*_{\alpha i} U_{\beta j} \langle \nu_j \mid \nu_i(t)\rangle \right|^2 \\ &= \delta_{\alpha\beta} - 4\sum_{i<j}^{n} \mathrm{Re}\left[U_{\alpha i}U^*_{\beta i}U^*_{\alpha j}U_{\beta j}\right] \sin^2 X_{ij} + 2\sum_{i<j}^{n} \mathrm{Im}\left[U_{\alpha i}U^*_{\beta i}U^*_{\alpha j}U_{\beta j}\right] \sin 2X_{ij}, \end{aligned} \tag{1.8}$$

where

$$X_{ij} = \frac{\left(m_i^2 - m_j^2\right) L}{4E} = 1.267 \frac{\Delta m^2_{ij}}{\mathrm{eV}^2} \frac{L/E}{\mathrm{m/MeV}}. \tag{1.9}$$

We have used the fact that the neutrinos are relativistic ($p >> m_i$) to make this simplification. Now, note that all the neutrino oscillation effects are encoded in the two mass-squared splittings ($\Delta m^2_{21} \equiv \left(m_2^2 - m_j^1\right)$ and $\Delta m^2_{31} \equiv (m_3^2 - m_1^2)$) and the 3×3 unitary matrix U. This matrix is parameterized in terms of three mixing angles $\theta_{12},\ \theta_{13},$

θ_{23} and a CP-violating Dirac phase δ_{CP} as

$$U = \begin{pmatrix} c_{12}c_{13} & s_{12}c_{13} & s_{13}e^{-i\delta_{\rm CP}} \\ -s_{12}c_{23} - c_{12}s_{13}s_{23}e^{i\delta_{\rm CP}} & c_{12}c_{23} - s_{12}s_{13}s_{23}e^{i\delta_{\rm CP}} & c_{13}s_{23} \\ s_{12}s_{23} - c_{12}s_{13}c_{23}e^{i\delta_{\rm CP}} & -c_{12}s_{23} - s_{12}s_{13}c_{23}e^{i\delta_{\rm CP}} & c_{13}c_{23} \end{pmatrix} \tag{1.10}$$

where $c_{ij} \equiv \cos\theta_{ij}$ and $s_{ij} \equiv \sin\theta_{ij}$. The value of these parameters as fit by the current neutrino oscillation data is tabulated in Table1.1[1].

Table 1.1: Neutrino oscillation from a 2020 global analysis of neutrino oscillation data. The $1\sigma, 2\sigma, 3\sigma$ ranges for both IO and NO are given.[1]

Parameter	Best fit $\pm 1\sigma$	2σ range	3σ range
$\Delta m^2_{21}[10^{-5}\text{eV}^2]$	$7.50^{+0.22}_{-0.20}$	7.12–7.93	6.94–8.14
$\lvert\Delta m^2_{31}\rvert[10^{-3}\text{eV}^2]$ (NO)	$2.55^{+0.02}_{-0.03}$	2.49–2.60	2.47–2.63
$\lvert\Delta m^2_{31}\rvert[10^{-3}\text{eV}^2]$ (IO)	$2.45^{+0.02}_{-0.03}$	2.39–2.50	2.37–2.53
$\sin^2\theta_{12}/10^{-1}$	3.18 ± 0.16	2.86–3.52	2.71–3.69
$\theta_{12}/$	34.3 ± 1.0	32.3–36.4	31.4–37.4
$\sin^2\theta_{23}/10^{-1}$ (NO)	5.74 ± 0.14	5.41–5.99	4.34–6.10
$\theta_{23}/$ (NO)	49.26 ± 0.79	47.37–50.71	41.20–51.33
$\sin^2\theta_{23}/10^{-1}$ (IO)	$5.78^{+0.10}_{-0.17}$	5.41–5.98	4.33–6.08
$\theta_{23}/$ (IO)	$49.46^{+0.60}_{-0.97}$	47.35–50.67	41.16–51.25
$\sin^2\theta_{13}/10^{-2}$ (NO)	$2.200^{+0.069}_{-0.062}$	2.069–2.337	2.000–2.405
$\theta_{13}/$ (NO)	$8.53^{+0.13}_{-0.12}$	8.27–8.79	8.13–8.92
$\sin^2\theta_{13}/10^{-2}$ (IO)	$2.225^{+0.064}_{-0.070}$	2.086–2.356	2.018–2.424
$\theta_{13}/$ (IO)	$8.58^{+0.12}_{-0.14}$	8.30–8.83	8.17–8.96
δ/π (NO)	$1.08^{+0.13}_{-0.12}$	0.84–1.42	0.71–1.99
$\delta/$ (NO)	194^{+24}_{-22}	152–255	128–359
δ/π (IO)	$1.58^{+0.15}_{-0.16}$	1.26–1.85	1.11–1.96
$\delta/$ (IO)	284^{+26}_{-28}	226–332	200–353

The neutrino oscillation parameters have a specific pattern that is worth elaborating on. The two mass-squared differences have a large hierarchy between them with their

ratio $|\Delta m^2_{21}/\Delta m^2_{31}| \sim 10^{-2}$. Depending on the absolute scale of neutrino masses, this can lead to a hierarchical or a quasi-degenerate mass pattern for the SM neutrinos. The mixing angles in the neutrino sector are in sharp contrast with the analogous mixing angles in the quark sector. While the quark mixing angles are very small, two of the neutrino mixing angles θ_{12}, and θ_{23} are large whereas the remaining angle θ_{13} is small. This peculiar pattern has inspired many models based on non-Abelian discrete symmetries such as A_4 which can approximately produce this pattern.

While the neutrino oscillation data has conclusively proven that the neutrinos are indeed massive, there are questions about the neutrino masses that these neutrino oscillation experiments cannot answer. Some of these important questions are

- *Absolute scale of neutrino masses :* As can be seen from Eq. (1.8), the neutrino oscillation probabilities only depend on the mass-squared splittings and not on the masses themselves. Since we have measured two non-vanishing mass splittings, we know that at least two of the SM neutrinos must be massive. However, the neutrino oscillation experiments cannot measure the mass of the lightest neutrino. Therefore, the absolute scale of the neutrino masses is unknown. It is convenient to parameterize this ignorance in terms of the sum of neutrino masses ($\sum m_\nu$).

- *Neutrino mass ordering :* The neutrino oscillation effects in the vacuum only depend on the *absolute* value of the mass squared splittings $|\Delta m^2_{ij}|$. We know that the sign of the splitting $\Delta m^2_{21} > 0$ because the matter effects in the Sun that affect the solar neutrino data depend on this sign. However, the sign of the larger mass splitting $|\Delta m^2_{31}|$ is unknown. This leads to two possibilities for neutrino mass ordering:

normal ordering (no) and inverted ordering (io). In normal ordering, the small mass splitting $|\Delta m^2_{21}|$ is between the two heavier neutrinos whereas in the inverted ordering, the small mass splitting $|\Delta m^2_{21}|$ is between the two lighter neutrinos.

- *Dirac/Majorana nature of SM neutrinos :* As we discussed before, the fermion masses in relativistic quantum field theory can be of the Dirac type or the Majorana type. Both these choices are viable for the SM neutrinos and therefore, neutrinos could be their anti-particles (Majorana) or not (Dirac). The current experimental data are not sensitive to this difference. Since a Majorana mass for neutrinos will violate lepton number by two units, the ongoing searches for the rare neutrinoless double beta decay process $(A,\ Z) \rightarrow (A,\ Z+2) + 2e^-$ is the best opportunity to answer this question.

Another fundamental question that is raised by the non-zero mass of neutrinos is their lifetime. The case for neutrino decay is theoretically extremely well-motivated. Neutrino decay is a characteristic feature of models in which neutrinos have masses. In quantum mechanics, any process that is not explicitly forbidden by symmetry or phase space considerations is expected to happen. For example, in the case of electrons, their stability is guaranteed by the conservation of electric charge, while for protons, their stability is owed to the conservation of the baryon number. In the SM, the baryon number and lepton number are accidental symmetries that are expected to be violated by BSM physics. This means that protons could be unstable in BSM models. In fact, one of the striking predictions of the well-motivated grand unified theories (GUT) is the existence of proton decay. Photons are stable, because being massless, their decay is forbidden by

phase space considerations. This argument also ensures stability for massless neutrinos in the SM. However, a massive neutrino has no such protection from decay. The flavor lepton numbers can in principle guarantee the stability for neutrinos but we know that the flavor lepton numbers are already broken in nature from the observation of flavor oscillations. With this perspective, it is most likely that neutrinos are unstable and have a finite lifetime. This makes the scenario of the decaying SM neutrino very well-motivated in light of its non-vanishing mass. In fact, neutrino decay is a characteristic feature of any model that is proposed to explain the light mass for neutrinos. The value of the neutrino lifetime in these models depends on the new physics that is responsible for the small neutrino mass.

Let us consider some explicit examples. Even in the minimal extensions of the SM that incorporate Dirac neutrino masses by adding right-handed neutrinos, or Majorana masses by including the non-renormalizable Weinberg operator, the heavier neutrinos undergo two-body decays at one loop into a lighter neutrino and a photon [2, 3, 4, 5, 6], (useful discussions may also be found in [7, 8]). In these scenarios, the lifetime of the massive neutrino is given by $\tau_\nu \sim 10^{50}\mathrm{s}\,(0.05\,\mathrm{eV}/m_\nu)^5$, assuming the daughter neutrino mass is negligible. This is much longer than the age of the universe, and therefore these minimal frameworks do not give rise to observable cosmological signals from neutrino decay. However, in more general extensions of the SM that incorporate neutrino masses, the neutrino lifetime can be much shorter. In particular, this includes theories in which the generation of neutrino masses is associated with the spontaneous breaking of global symmetries in the neutrino sector [9, 10, 11, 12, 13], (see also [14, 15]). The SSB of these symmetries will result in (light) massless (pseudo-) Goldstone bosons that have off-

diagonal couplings to neutrinos, such that it connects fermions of non-identical masses. In this framework, the heavier neutrinos can decay into a lighter neutrino and one of the Goldstone bosons associated with the spontaneous breaking of the global symmetry. In this case, the strength of this $\bar{\nu}_i n_j \phi$ coupling is given by m_ν / f from dimensional considerations where f is the scale at which SSB occurs. This factor could be small enough to evade the current constraints from astrophysical sources but still be large enough to have effects in cosmology. The neutrino lifetime in these models can be shorter than or comparable to the age of the universe for a wide range of values of scales f. In this framework, the heavier neutrinos can decay into a lighter neutrino and one of the Goldstone bosons associated with the spontaneous breaking of the global symmetry. The timescale for this process can be shorter than or comparable to the age of the universe, giving rise to cosmological signals. In general, neutrinos that are unstable on cosmological timescales remain an intriguing possibility due to the strong motivations for new physics that explains the smallness of neutrino masses.

In the past, the decaying neutrino scenario has been explored as a solution to the solar and atmospheric neutrino problems [16, 17, 18, 19]. However, the resulting predictions for the energy spectrum of the solar neutrinos and the decay lengths required for this proposal are now disfavored by the data [20, 21, 22]. There has also been earlier work studying the impact of the decay of massive neutrinos on structure formation [23, 24]. However the range of parameter space that was considered is much above the current limits on the masses of the neutrinos. More recently, radiative neutrino decays have been proposed as an explanation of the 21 cm signal observed by the EDGES experiment [25].

The current limits on the neutrino lifetime are rather weak, except in the case of

decays to final states involving photons. In this specific case, the absence of spectral distortions in the cosmic microwave background (CMB) places strong bounds on radiative decays from a heavier neutrino mass eigenstate to a lighter one, $\tau_\nu \gtrsim 10^{19}$s for the larger mass splitting and $\tau_\nu \gtrsim 4 \times 10^{21}$s for the smaller one [26]. There are also very strong, albeit indirect, limits on radiative neutrino decays based on the tight laboratory and astrophysical bounds on the neutrino dipole moment operators that induce this process [27, 28, 29, 30, 31].

In contrast, the decay of neutrinos into dark radiation that does not possess electromagnetic interactions is only weakly constrained by current cosmological, astrophysical, and terrestrial data. The most stringent bound on this scenario arises from CMB measurements. If neutrino decay and inverse decay processes are effective during the CMB epoch, they prevent the neutrinos from free streaming, leading to observable effects on the CMB [32, 33, 34]. Current measurements of the CMB power spectra require neutrinos to free stream from redshifts $z \approx 8000$ until recombination, $z \approx 1100$ [35, 36, 37, 38].[1] This can be used to set a lower bound on the neutrino lifetime $\tau_\nu \geq 4 \times 10^8\,\mathrm{s}\,(m_\nu/0.05\,\mathrm{eV})^3$ for SM neutrinos decaying into massless dark radiation [38]. Several astrophysical observations have also been used to set limits on the neutrino lifetime. However, the resulting bounds are much weaker. The observation that the neutrinos emitted by Supernova 1987A did not decay prior to reaching the earth can be used to set a bound on the lifetime of the electron-neutrino, $\tau_{\nu_e}/m_{\nu_e} \geq 5.7 \times 10^5\,\mathrm{s/eV}$ [40]. Similarly, the detection of solar neutrinos at the earth can be used to place a bound on the lifetime of the mass eigenstate ν_2, $\tau_\nu/m_\nu \gtrsim 10^{-4}\,\mathrm{s/eV}$ [22, 41, 42]. Limits on the neutrino lifetime can also be obtained

[1] Also see the more recent discussion in [39] for the effects of interacting neutrinos on the CMB.

from atmospheric neutrinos and long-baseline experiments, but the resulting constraints are even weaker (see e.g. [43, 44, 45, 46]). Therefore, at present there is no evidence that neutrinos are stable on cosmological timescales, and that the cosmic neutrino background (CνB) has not decayed away into dark radiation.

At present, the strongest limit on the sum of neutrino masses, $\sum m_\nu < 0.12$ eV, is from cosmological observations [47]. These measurements are sensitive to the neutrino masses through the gravitational effects of the relic neutrinos left over from the Big Bang. In determining the size of this effect [48, 49], (reviews with additional references may be found in [50, 51, 52, 53]), it is assumed that the neutrinos are stable on timescales of order the age of the universe.

In particular, if the neutrino lifetime is less than the age of the universe [54, 55], or if the neutrinos have annihilated away into lighter states [56, 57], this bound on the neutrino masses is no longer valid and must be reconsidered. In this dissertation, we explore the cosmological signals that arise from a general framework in which the neutrinos decay into dark radiation on timescales shorter than the age of the universe. We determine the bound on the sum of neutrino masses and explore the prospects of measuring the neutrino lifetime using cosmological datasets. Our focus is on the case in which neutrinos decay after becoming non-relativistic. This dissertation is based on the papers [58, 59].

The impact of non-vanishing neutrino masses on cosmological structure formation is well understood, (see [50, 51] for useful reviews).

- Sub-eV neutrinos constitute radiation at the time of matter-radiation equality. Therefore, fluctuations about the background neutrino number density do not contribute significantly

to the growth of structure until after neutrinos have become non-relativistic. Consequently, perturbations on scales that enter the horizon prior to neutrinos becoming non-relativistic evolve differently than scales that enter afterwards, thereby affecting the matter power spectrum.

- After neutrinos become non-relativistic, their overall contribution to the energy density redshifts away less slowly than that of a relativistic species of the same abundance. This results in a larger Hubble expansion, reducing the time available for structure formation. This leads to an overall suppression of Large Scale Structure (LSS).

Then the leading effect of non-vanishing neutrino masses is to suppress the growth of structure on scales that entered the horizon prior to the neutrinos becoming non-relativistic. The extent of this suppression depends on the values of the neutrino masses. Since heavier neutrinos become non-relativistic earlier and also contribute a greater fraction of the total energy density after becoming non-relativistic, a larger neutrino mass leads to a larger suppression of LSS. In the case of neutrinos that decay, this suppression now also depends on the neutrino lifetime. After neutrinos have decayed, their contribution to the energy density redshifts like that of massless neutrinos, resulting in a milder suppression of structure as compared to stable neutrinos of the same mass. It follows that there is a strong degeneracy between the neutrino mass and the lifetime inferred from the matter power spectrum. The cosmological upper bound on the neutrino mass is therefore lifetime-dependent, as was first discussed in [54, 55].

Neutrino masses also lead to observable effects on the CMB. Sub-eV neutrinos

become non-relativistic after CMB decoupling. The main "primary" effect on the CMB is through the early and late integrated-Sachs-Wolfe effects, as well as a modification of the angular diameter distance to the last scattering surface. Because of their impact on the growth of structure detailed above, neutrinos also affect the CMB through the "secondary" effect of lensing. At the precision of Planck, the effects of lensing drive the CMB constraints on the sum of neutrino masses. Since neutrino decay results in a milder suppression of structure as compared to stable neutrinos of the same mass, the bounds on $\sum m_\nu$ from CMB lensing are also lifetime dependent.

From the discussion above, we find the the cosmological sensitivity to neutrino mass arises from the physics that happen after neutrinos have become non-relativistic. The effect of massive neutrinos is to suppress all the modes that enter the horizon after the neutrinos turn non-relativistic. In order for the neutrino decay to make an effect on these signals, the decay should happen after the neutrinos turn non-relativstic. This corresponds to the width $\Gamma_\nu \lesssim 1 \times 10^5 (m_\nu/0.1\,\mathrm{eV})^{3/2}$ km/s/Mpc for each neutrino. In this regime, we can also neglect the inverse-decay processes as this process is not efficient. If neutrinos decayed, this suppression will be decreased leading to a degeneracy between the neutrino lifetime and the neutrino mass. In order for the decay scenario to make the maximum deviation from the massive and massless neutrino scenarios, we need the daughter particles to be as light as possible. Our focus in this dissertation is on the decay of neutrinos to dark radiation, since this framework has a greater impact on the bound on $\sum m_\nu$ than the decay of heavier neutrinos to lighter ones. In particular, at present the cosmological limits on $\sum m_\nu$ only constrain quasi-degenerate neutrino spectra, so that decays of heavier neutrinos to lighter ones are not expected to alter the current bound

significantly.

We have, therefore, two reasons to consider the unstable neutrino scenario in cosmology especially the regime in which neutrinos decay into radiation after becoming non-relativistic. Firstly, the cosmological neutrino mass bound is lifetime dependent. This bound can be significantly relaxed, as we find if neutrinos are unstable thus opening up a range of neutrino masses that is important for terrestrial experiments. Secondly, the lifetimes of SM neutrinos are fundamental parameters of particle physics. Cosmology may be the only avenue to detect this decay if neutrinos decay into dark radiation with a lifetime comparable to the age of the universe.

We begin our analysis by deriving the Boltzmann equations that govern the cosmological evolution of density perturbations in the case of unstable neutrinos. We then appropriately modify the Boltzmann code CLASS[2] [60] to calculate the CMB and matter power spectra to accommodate this framework. We find that the results admit a simple analytic understanding. We then perform a Monte Carlo analysis based on CMB and LSS data (Planck+BAO+Pantheon+LSS) to determine the bounds on this scenario. We use the likelihood function from the Planck 2015 analysis [61]. We find that when the stable neutrino assumption is relaxed, the limits on the neutrino masses from this data set become much weaker, with the bound on $\sum m_\nu$ increasing from 0.25 eV to 0.9 eV. Importantly, this shows that the cosmological bounds do not exclude the region of parameter space in which future experiments such as KATRIN [62], KamLAND-ZEN (KLZ) [63] and the Enriched Xenon Observatory (EXO) [64, 65] are sensitive to the neutrino masses.

In the coming decade, major improvements are expected in the precision of cosmological

[2]http://www.class-code.net

observations, which would lead to great advances in neutrino physics. The Euclid satellite, scheduled to be launched in 2022, is expected to measure both the galaxy and the cosmic shear power spectra with unprecedented precision, achieving up to sub-percent accuracy over the redshift range from $z \sim 0.5 - 2$ [66]. In the more distant future, the CMB-S4 experiment [67] will lead to major advances over current CMB observations. This includes improvements in the measurement of CMB lensing, which is very sensitive to the neutrino masses. Under the assumption that neutrinos are stable, these new measurements will allow us to probe values of the neutrino masses smaller than the observed neutrino mass splittings and thereby determine $\sum m_\nu$ [68, 69]. However, if the neutrinos are unstable on cosmological timescales, the question of whether $\sum m_\nu$ can in fact be determined remains unanswered. We show that in this case of non-relativistic decay of neutrinos into dark radiation, near-future large scale structure (LSS) measurements from Euclid, in combination with Planck data, may allow an independent determination of both the lifetime of the neutrinos and the sum of their masses. The reason these parameters can be independently determined is because Euclid takes measurements at multiple redshifts, which allows us to track the growth of structure over time. In the case of stable neutrinos, we find that these observations will be able to extend the lower bound on the lifetime by at least seven orders of magnitude, from $\mathcal{O}(10)$ years to $\mathcal{O}(0.1 - 10)$ Gyrs depending on the neutrino mass, without significantly affecting the measurement of the sum of neutrino masses. Furthermore, we show that if the neutrinos decay after becoming non-relativistic but with a lifetime of less than $\mathcal{O}(10^8)$ years, these observations may allow the first determination of not just the neutrino masses, but also the neutrino lifetime.

The outline of this dissertation is as follows. In the next chapter, we will discuss

how to implement the non-relativistic neutrino decay in the framework of kinetic theory in the expanding universe and understand its implications in light of the current cosmological data. In section 2.1, we discuss the parameter space of the neutrino mass and lifetime, outlining the current bounds. In section 2.2, we derive the Boltzmann equations that dictate the cosmological evolution of perturbations in the phase-space distribution of unstable neutrinos and their daughter radiation. While our focus is on the case in which the decaying particles are neutrinos, the formalism is more general and can be applied to the much larger class of models in which warm dark matter decays into dark radiation. In section 2.3.1, we numerically compute the growth of perturbations in the case of unstable neutrinos and determine the effects on the matter power spectrum and CMB lensing. To obtain a physical understanding, in section 2.3.2 we derive analytical expressions for these effects. In section 2.4, we perform a Monte Carlo scan of the parameter space and derive constraints on the mass and lifetime of the neutrino from current data.

In chapter 3, we study the prospects of an independent detection of neutrino mass and lifetime from future experiments such as Euclid and CMB S4. In section 3.1, we discuss how the red-shift evolution of perturbations can be used to distinguish between two $(\sum m_\nu, \Gamma_\nu)$ scenarios that are degenerate in the context of current data. In section 3.2, we do an MCMC analysis using mock Euclid and CMB S4 likelihoods to obtain the region of parameter space where these experiments can independently measure the neutrino mass and lifetime. Using this, we also obtain the prospective future bound on the neutrino lifetime from these experiments if neutrinos are stable on timescales of order of the age of the universe. For some $(\sum m_\nu, \Gamma_\nu)$ benchmark points, we also show the prospective 95% and 68% C.L. intervals for $(\sum m_\nu, \Gamma_\nu)$ as expected to be measured by

these experiments.

In appendix A we present an example of a simple model in which the neutrinos decay into dark radiation on timescales of order the age of the universe. This model is consistent with all current cosmological, astrophysical, and laboratory bounds, and represents a concrete realization of the scenario we are considering. However, we stress that the results presented in the body of the dissertation are not restricted to this specific model, but apply to any theory in which the neutrinos decay to dark radiation after becoming nonrelativistic.

Chapter 2: Current Limits on Neutrino Mass and Lifetime from Cosmology

2.1 Parameter Space of the Unstable Neutrino

In this section we outline the constraints on the decay of neutrinos to dark radiation. As explained in the introduction, these bounds only place limits on a combination of the neutrino mass and the lifetime. Therefore, in this study we will map out the constraints and the signals in the two-dimensional parameter space spanned by the sum of neutrino masses ($\sum m_\nu$) and the neutrino decay width (Γ_ν), as displayed in Fig. 2.1. In our analysis we make the simplifying assumption that all three neutrinos are degenerate in mass. As we shall see, the bounds on $\sum m_\nu$ are always much larger than the observed mass splittings, and so this is an excellent approximation in the relevant parameter space. We further assume that all three neutrinos have the same decay width Γ_ν. Since the mixing angles in the neutrino sector are large, this is a good approximation in many simple models of decaying neutrinos if the spectrum of neutrinos is quasi-degenerate. In particular, the model presented in appendix A exhibits this feature.

There is a hard lower limit on the sum of neutrino masses from the atmospheric and solar mass splittings which constrain $\sum m_\nu \geq \sqrt{\Delta m^2_{31}} + \sqrt{\Delta m^2_{21}} = 0.06$ eV in the case of normal ordering and $\sum m_\nu \geq 2 \times \sqrt{\Delta m^2_{31}} = 0.1$ eV in the case of inverted ordering [70]. Therefore, we present the parameter space starting from $\sum m_\nu = 0.06$

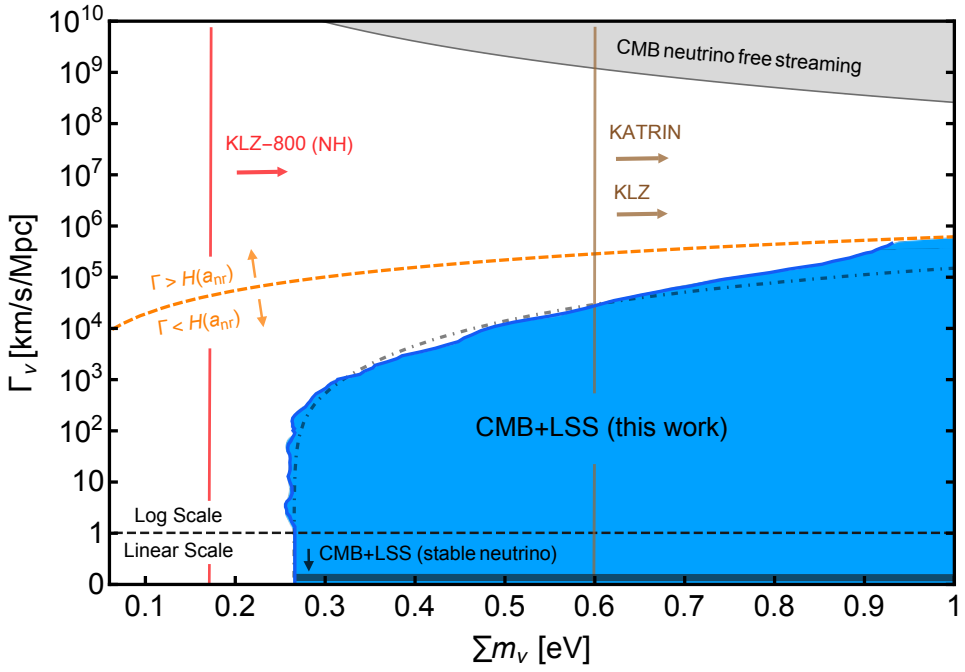

Figure 2.1: The plot shows the current constraints in the $\sum m_\nu - \Gamma_\nu$ parameter space. The colored regions are excluded by current data while the white region is allowed. The orange dashed line separates the region of parameter space in which neutrinos decay while still relativistic from that in which they decay after becoming non-relativistic. Our study focuses on the region below this line, corresponding to the latter scenario. The light grey regions show current constraints on neutrino mass and lifetime coming from CMB free streaming and the bound on stable neutrinos (labelled "CMB+LSS (stable neutrino)"). Our analysis excludes the blue region labelled "CMB+LSS (this work)" based on CMB and LSS data (Planck+BAO+Pantheon+LSS). The dash-dotted line represents the approximate constraint obtained by simply requiring that the matter power spectrum be consistent with observations in the neighborhood of $k = 0.1\,h$/Mpc with fixed H_0. This is seen to provide a reasonable estimate to the constraints from all data. The vertical brown band shows the projected KATRIN sensitivity and also the current KLZ sensitivity. The vertical red line shows the projected KLZ-800 sensitivity in the case of a normal hierarchy.

eV. CMB observations can be used to obtain an upper bound on the sum of neutrino masses. The current CMB data constrains the effective number of neutrinos, $N_{\rm eff}$, during the epoch of acoustic oscillations to be 2.99 ± 0.17 [47], which is perfectly compatible with the SM value of 3.046. Then, if neutrinos are stable on CMB timescales, we can obtain an approximate upper bound on their masses by requiring that all three species of neutrinos are relativistic at recombination. This translates into an approximate limit, $\sum m_\nu \lesssim 3T_{\rm rec} \approx 0.9$ eV. A more precise bound can be obtained from a fit to the CMB data.

The CMB can also be used to constrain the masses of neutrinos that decay prior to recombination. As mentioned in the introduction, CMB data requires the species that constitute $N_{\rm eff}$ to be free streaming at redshifts below $z \approx 8000$ until recombination, $z \approx 1100$. This can be used to place limits on processes such as neutrino decays and inverse decays that prevent neutrinos from free streaming at late times. The resulting bound depends on the neutrino mass, and is given by $\tau_\nu \geq 4 \times 10^8\,\mathrm{s}\,(m_\nu/0.05\,\mathrm{eV})^3$ [38]. This bound excludes the grey region at the top of Fig. 2.1. Naively, one might expect the CMB bounds from free streaming to rule out all theories in which the neutrino decays before recombination, independent of the neutrino mass. However, in the case of an ultrarelativistic mother particle, the decay process results in approximately collinear daughter particles moving in the same direction as the mother. Similarly the inverse decay process generally only involves collinear initial state particles, so that there is no significant disruption in the flow of energy even if the decay and inverse decay processes are efficient [35]. The net constraint from CMB free streaming is therefore much weaker on the decays of light neutrinos.

As discussed in the introduction, massive neutrinos suppress the growth of matter perturbations by reducing the time available for structure formation. In the case of stable neutrinos, this has been used to set a constraint on the sum of neutrino masses, $\sum m_\nu \leq 0.12$ eV [47]. Unstable neutrinos that decay after becoming non-relativistic also lead to a suppression in the growth of structure that now depends on the neutrino lifetime. In this dissertation, we determine the resulting bound in the two dimensional parameter space spanned by $\sum m_\nu$ and the neutrino lifetime. Based on the Monte Carlo study presented in Sec. 2.4, CMB and LSS data (Planck+BAO+Pantheon+LSS) exclude the blue region labelled as "CMB+LSS (this work)" in Fig. 2.1. We have scanned the region between $0 \leq \log_{10}\frac{\Gamma_\nu}{\text{km/s/Mpc}} \leq 5.5$. In Fig. 2.1, we simply extrapolate the bound at $\log_{10}\frac{\Gamma_\nu}{\text{km/s/Mpc}} = 0$ to $\Gamma_\nu = 0$, because the constraint on $\sum m_\nu$ is independent of Γ_ν when $\Gamma_\nu \ll H_0$. The existing constraint on the masses of stable neutrinos from this data set forms the lower boundary of this region (labelled as "CMB+LSS (stable neutrino)").

The dash-dotted line that approximately envelopes the blue shaded region represents the constraint obtained by simply requiring that the matter power spectrum be consistent with observations in the neighborhood of $k = 0.1\,h$/Mpc with fixed H_0, where the current LSS measurements have the best sensitivity. We see that it provides a good approximation to the true bound, except in the region of $\sum m_\nu \gtrsim 0.9$ eV, where the CMB limits on $N_{\rm eff}$ at recombination become important. The impact of neutrinos on the matter power spectrum depends slightly on the mass ordering as the individual mass eigenstates become non-relativistic at different times. However, since the current limits are only sensitive to quasi-degenerate spectra, we are justified in neglecting this effect.

The orange dashed line ($\Gamma = H(z_{\rm nr})$) separates the region where neutrinos decay

when non-relativistic from the region where they decay while still relativistic. Here $z_{\rm nr}$, the approximate redshift at which neutrinos become non-relativistic, is defined implicitly from the relation $3T_\nu(z_{\rm nr}) = m_\nu$. This definition is based on the fact that for relativistic neutrinos at temperature T_ν, the average energy per neutrino is approximately $3T_\nu$. The Hubble scale at $z_{\rm nr}$ is given by,

$$\begin{aligned} H(z_{\rm nr}) &= H_0\sqrt{\Omega_m}\Big(\frac{\sum m_\nu}{9T_\nu^0}\Big)^{3/2} \\ &\simeq 7.5\times10^5{\rm km/s/Mpc}\Big(\frac{H_0}{68{\rm km/s/Mpc}}\Big)\Big(\frac{\Omega_m}{0.3}\Big)^{1/2}\Big(\frac{\sum m_\nu}{1{\rm eV}}\Big)^{3/2}\Big(\frac{1.5\times10^{-4}{\rm eV}}{T_\nu^0}\Big)^{3/2}. \end{aligned} \tag{2.1}$$

Since our study assumes neutrinos decay after they become non-relativistic, we only present the constraints below this orange dashed line.

The currently allowed parameter space is represented by the white regions in Fig. 2.1. In the white region above the orange dashed line, even though neutrinos decay when still relativistic, their small mass allows them to evade the current CMB free streaming constraints. In this scenario their contribution to the energy density evolves in a manner similar to that of massless neutrinos, and so the effects on LSS are similar in the two cases. In the white region below the orange dashed line the neutrinos decay after becoming non-relativistic, but because their masses are too small or their lifetimes too short, the suppression of the matter power spectrum is too small to be detected with current data.

We see from this discussion that the unstable neutrino paradigm greatly expands the range of neutrino masses allowed by current data. This has important implications for current and future laboratory experiments designed to detect neutrino masses. Next generation tritium decay experiments such as KATRIN [62] are expected to be sensitive

to values of m_{ν_e} as low as 0.2 eV, corresponding to $\sum m_\nu$ of order 0.6 eV. A signal in these experiments would conflict with the current cosmological bound, $\sum m_\nu < 0.12$ eV, for stable neutrinos. However, in the decaying neutrino paradigm, we have seen that the current cosmological upper bound on the sum of neutrino masses is relaxed, with the result that $\sum m_\nu$ as high as 0.9 eV is still allowed. Therefore, a signal at KATRIN can be accommodated if neutrinos are unstable on cosmological timescales. In Fig. 2.1, we display a brown vertical line $\sum m_\nu \approx 0.6$ eV that corresponds to the expected KATRIN sensitivity.

In the case of Majorana neutrinos, current data from neutrinoless double-beta decay experiments such as KLZ and EXO have already ruled out $\sum m_\nu \gtrsim 0.6$ eV (brown vertical line) [63, 65]. An updated version of KLZ, the KLZ-800, is currently probing $\sum m_\nu$ as low as 0.17 eV [71] (red vertical line) in the case of the normal hierarchy and the entire parameter space for the inverted hierarchy. If this experiment were to see a signal, we cannot immediately conclude that hierarchy is inverted based on the current cosmological bound of $\sum m_\nu < 0.12$ eV, since the decaying neutrino paradigm would still admit a normal hierarchy.

2.2 Evolution of Perturbations in the Decay of Non-Relativistic Particles into Radiation

In this section we derive the set of Boltzmann equations describing the evolution of the phase-space density of massive particles decaying into massless daughter particles, working to first order in the perturbations. In contrast to the case of cold dark matter

(CDM) decay (see, e.g., [72, 73]), we cannot assume that the mother particles are at rest, but must take into account their non-trivial momentum distribution, as in the studies [74, 75, 76]. This allows us to study the cosmological effects of a warm particle species, such as neutrinos or warm dark matter, decaying into radiation. We implement these new Boltzmann equations into the numerical code CLASS to generate the results in sections 2.3.1 and 2.4.

The phase-space distribution of a particle species in the expanding universe is a function of the position $\vec{x}$, the comoving momentum $\vec{q} \equiv q\hat{n}$, and the comoving time τ. The evolution of this distribution is determined by the Boltzmann equation,

$$\frac{df}{d\tau} = \frac{\partial f}{\partial \tau} + \frac{dx^i}{d\tau}\frac{\partial f}{\partial x^i} + \frac{dq}{d\tau}\frac{\partial f}{\partial q} + \frac{d\hat{n}}{d\tau}.\frac{\partial f}{\partial \hat{n}} = C[f] \,, \tag{2.2}$$

where $C[f]$ is the collision term that accounts for all processes involving the species.

We consider the case of a massive mother (with the subscript M for mother) of mass M decaying into N daughters ($D_{i=1,2...N}$). For the sake of simplicity, we restrict ourselves to the case where the mother particles decay after becoming non-relativistic, but nevertheless keep track of their non-trivial momentum distribution. In this regime, inverse-decay processes can be safely neglected. We also ignore any effects arising from Pauli blocking and spontaneous emission since $f_{M,Di} \ll 1$. The collision terms for the mother and daughter particles are then given by,

$$C_M = \; - \; \frac{a^2}{2\epsilon_M} \int \prod_i \frac{\bar{d}^3\vec{q}_i}{2\epsilon_{Di}} |\mathcal{M}|^2 (2\pi)^4 \delta^{(4)}(\vec{q}_M - \Sigma_i \vec{q}_{Di}) f_M(q_M), \tag{2.3}$$

$$C_{Dj} = \quad + \quad \frac{a^2}{2\epsilon_{Dj}} \int \frac{\bar{d}^3\vec{q}_M}{2\epsilon_M} \prod_{i \neq j} \frac{\bar{d}^3\vec{q}_i}{2\epsilon_{Di}} |\mathcal{M}|^2 (2\pi)^4 \delta^{(4)}(\vec{q}_M - \Sigma_i \vec{q}_{Di}) f_M(q_M). \quad (2.4)$$

where $\epsilon_S \equiv (q_S^2 + m_S^2 a^2)^{1/2}$ represents the comoving energy of the species $S(\equiv M, D_i)$ and $\bar{d}^3\vec{q} \equiv d^3\vec{q}/(2\pi)^3$. From the definition of the decay width, the collision term for the mother particle can be simplified to

$$C_M = -\frac{a\Gamma}{\gamma} f_M, \quad (2.5)$$

where Γ denotes the decay width in the rest frame of the decaying particle, and the relativistic boost factor $\gamma \equiv \sqrt{q_M^2 + M^2 a^2}/(Ma)$ accounts for time-dilation in the cosmic frame. To determine the evolution of inhomogeneities in our universe, we consider perturbations about the homogeneous and isotropic background phase space distribution functions,

$$f_S(q_S, \hat{n}, \vec{x}, \tau) \quad = \quad f_S^0(q_S, \tau) + \Delta f_S(q_S, \hat{n}, \vec{x}, \tau), \quad S = M, D_i. \quad (2.6)$$

2.2.1 Background: Zeroth Order

Treating Δf_M and fluctuations about the gravitational background as higher order perturbations, the zeroth order Boltzmann equations for f_M^0 arising from Eq. (2.2) take the form,

$$\frac{\partial f_M^0}{\partial \tau} \quad = \quad -a\frac{\Gamma}{\gamma} f_M^0. \quad (2.7)$$

The formal solution to $f_M^0(q,\tau)$ from the differential equations in Eq. (2.7) is given by,

$$f_M^0(q,\tau) = f_i(q) e^{-\Gamma \int_{\tau_i}^{\tau} \frac{a}{\gamma(a)} d\tau'}, \tag{2.8}$$

where τ_i denotes the initial conformal time and $f_i(q)$ represents the initial momentum distribution. We will focus on the case where the mother decays after becoming non-relativistic. Using integration by parts, the exponent in Eq. (2.8) can be rewritten as,

$$\Gamma \int_{\tau_i}^{\tau} \frac{a\, d\tau'}{\gamma(a)} = \frac{\Gamma t'}{\gamma(a)}\bigg|_{t_i}^{t} - \Gamma \int_{t_i}^{t} dt'\, t' \frac{d}{dt'}\left(\frac{1}{\gamma(a)}\right), \tag{2.9}$$

where we have used $a d\tau = dt$. It is computationally demanding to solve the integral for general $a(\tau)$. However, the behavior of the exponential factor is rather simple: the exponential is close to 1 when τ is smaller than the mother lifetime $\sim \gamma/\Gamma a$, and f_M no longer contributes when τ is much larger than the mother lifetime. The only time that the exponential factor exhibits a non-trivial a-dependence is when $\tau \sim \gamma/\Gamma a$. Since our focus is on decays in the non-relativistic regime, $\gamma(a)$ is slowly varying at the time of decay. Then the second term on the right-hand side of Eq. (2.9), which depends on the time derivative of $\gamma(a)$, can be neglected in favor of the first term. This allows us to approximate the exponent as

$$\Gamma \int_{\tau_i}^{\tau} \frac{a\, d\tau'}{\gamma(a)} \approx \frac{\Gamma t}{\gamma(a)}. \tag{2.10}$$

We have verified numerically that Eq. (2.10) is a good approximation to the full solution. Therefore, the mother distribution we use in this dissertation is

$$f_M^0(q,\tau) \approx f_i(q) e^{-\frac{\Gamma}{\gamma(a)}t}. \tag{2.11}$$

It is worth pointing out that the mother distribution described by Eq. (2.11) is a general formula that can also be applied to the case of decaying CDM. This limiting case corresponds to the distribution $f_i(q_M) = \delta(q_M) N_{Mi}/(4\pi q_M^2)$, where N_{Mi} represents the initial comoving number density of mother particles. Since this distribution is localized entirely at $q_M = 0$, the boost factor $\gamma(a) = 1$. Then Eq. (2.11) reduces to the known result for decaying cold dark matter [77, 78, 79]. Our analysis is, however, more general, because it accounts for the fact that the contribution of warm dark matter to the background energy density scales with the redshift in a more complicated manner than a^{-3}. In addition, it takes into account the fact that, in general, particles with larger momenta live longer as a consequence of time dilation.

We now apply the above general formula to the decay of massive neutrinos. The SM neutrinos decoupled from the photon bath when they were ultra-relativistic. Therefore, their distribution prior to decay is of the Fermi-Dirac form. Therefore, $f_i = 1/(e^{q/T_{\nu 0}}+1)$, leading to

$$f_M^0 = \frac{1}{e^{q/T_{\nu 0}}+1} \exp(-\frac{\Gamma}{\gamma}t). \tag{2.12}$$

The collision terms for the daughter particles are more challenging. However, we can simplify this set of equations by using the total integrated Boltzmann equations for the

daughters. This is done by integrating the Boltzmann equations for the individual daughter species with respect to $\bar{d}^3\vec{q}_{Di}\epsilon_{Di}$ and adding them up. The resulting total integrated collision term for the daughter species is given by,

$$\begin{aligned}\sum_j \int \bar{d}^3\vec{q}_{Dj}\epsilon_{Dj}C^0_{Dj} &= a^2\int \frac{\bar{d}^3\vec{q}_M}{2\epsilon_M}\prod_i \frac{\bar{d}^3\vec{q}_{Di}}{2\epsilon_{Di}}(\sum_j \epsilon_{Dj})|\mathcal{M}|^2(2\pi)^4\delta^{(4)}(\vec{q}_M-\Sigma_i\vec{q}_{Di})f^0_M(q_M),\\ &= a^2\Gamma M\int \bar{d}^3\vec{q}_M f^0_M. \end{aligned} \tag{2.13}$$

The simplification in the last line follows from the covariant conservation of the energy-momentum tensor, where we have used Eq. (2.3), Eq. (2.5), and $\epsilon_M/\gamma = Ma$ to obtain this expression. In this work we focus on the case in which the mother neutrino decays into massless daughter particles. The relation in Eq. (2.13) can be used to express the Boltzmann equation for the daughters in terms of the total comoving energy density of the daughters E_D and the comoving number density of the mother N_M

$$E_D \equiv \sum_i \int dq_{D_i} q^3_{D_i} f_{D_i}, \qquad N_M \equiv \int dq_M q^2_M f_M\,. \tag{2.14}$$

Since the daughter particles constitute massless radiation, we can rewrite the expression for the evolution of the daughter distribution in Eq. (2.2) in terms of the background daughter energy density $\bar{\rho}_D \equiv 4\pi a^{-4}E^0_D$ and the background mother number density $\bar{n}_M \equiv 4\pi a^{-3}N^0_M$, where E^0_D and N^0_M are defined as in Eq. (2.14) after expanding out f_M and f_{D_i} as in Eq. (2.6),

$$\frac{\partial\bar{\rho}_D}{\partial\tau} + 4aH\bar{\rho}_D = a\Gamma M\bar{n}_M. \tag{2.15}$$

The right-hand side of the Eq. (2.15) is exactly the same as in the case of cold dark matter decay. While mother particles that have higher momentum have more energy, they also decay more slowly due to time-dilation in the cosmic frame. This perfect cancellation between relativistic energy and time-dilation is neatly encapsulated in the simplification $\epsilon_M/\gamma = Ma$ that was used in obtaining Eq. (2.13).

2.2.2 Perturbations: First Order

In the synchronous gauge, the metric perturbations can be parametrized as,

$$ds^2 = a(\tau)^2 \left[-d\tau^2 + (\delta_{ij} + H_{ij})\, dx^i dx^j\right], \tag{2.16}$$

where $d\tau = dt/a(\tau)$ and the indices i and j run over the three spatial coordinates, $(i, j = 1, 2, 3)$. It is convenient to work in Fourier space,

$$H_{ij}(\vec{k}, \tau) = \hat{k}_i \hat{k}_j h(\vec{k}, \tau) + \left(\hat{k}_i \hat{k}_j - \frac{1}{3}\delta_{ij}\right) 6\eta(\vec{k}, \tau)\ , \tag{2.17}$$

where $\vec{k}$ is conjugate to $\vec{x}$ and $\hat{k}$ is the unit vector. In Fourier space the first order terms in Eq. (2.2) for the mother particle can be collected as,

$$\Delta f_M' + i\frac{qk}{\epsilon_M} P_1(\mu) \Delta f_M + q\frac{\partial f_M^0}{\partial q}[-\frac{h'}{6} - \frac{P_2(\mu)}{3}(h' + 6\eta')] \;\; = \;\; -a^2 \frac{\Gamma M}{\epsilon_M} \Delta f_M,$$

(2.18)

where $\mu \equiv \hat{k} \cdot \hat{n}$ and $P_l(\mu)$ are the Legendre polynomials.

As usual, we can expand the angular dependence of the perturbations as a series in Legendre polynomials,

$$X(..., \vec{k}, \hat{n}) = \sum_{l=0}^{\infty} (-i)^l (2l+1) X_l(..., k) P_l(\hat{k} \cdot \hat{n}). \tag{2.19}$$

Here X represents any of the perturbations $\Delta f_{M,D_j}$, ΔE_D or ΔN_M, which are defined as in Eqs. (2.6) and (2.14). Exploiting the orthonormality of the Legendre polynomials, we arrive at a Boltzmann hierarchy of moments in which any moment is related only to its neighboring moments. The diminishing importance of the higher moments allows us to cutoff the calculation at some $l = l_{max}$, where the choice of l_{max} depends on our desired level of accuracy. We use the improved truncation scheme from Ref. [80], which has been generalized to spatial curvature in Ref. [81].

The Boltzmann hierarchy for the perturbations of the mother particle becomes,

$$\begin{aligned}
\Delta f'_{M(0)} &= -\frac{qk}{\epsilon_M} \Delta f_{M(1)} + \frac{h'}{6} q \frac{\partial f^0_M}{\partial q} - \frac{a^2 \Gamma M}{\epsilon_M} \Delta f_{M(0)}, \\
\Delta f'_{M(1)} &= \frac{qk}{3\epsilon_M} (\Delta f_{M(0)} - 2\Delta f_{M(2)}) - \frac{a^2 \Gamma M}{\epsilon_M} \Delta f_{M(1)}, \\
\Delta f'_{M(2)} &= \frac{qk}{5\epsilon_M} (2\Delta f_{M(1)} - 3\Delta f_{M(3)}) - (\frac{1}{15} h' + \frac{2}{5} \eta') q \frac{\partial f^0_M}{\partial q} - \frac{a^2 \Gamma M}{\epsilon_M} \Delta f_{M(2)}, \\
\Delta f'_{M(l)} &= \frac{qk}{(2l+1)\epsilon_M} [l \Delta f_{M(l-1)} - (l+1) \Delta f_{M(l+1)}] - \frac{a^2 \Gamma M}{\epsilon_M} \Delta f_{M(l)}, \quad l \geq 3.
\end{aligned} \tag{2.20}$$

In the limit that the decay term is set to zero, these equations reduce to the standard equations for massive neutrinos in the synchronous gauge [80], as expected.

For the Boltzmann hierarchy of daughter particles, we integrate with respect to $\int đ^3\vec{q}_{D_j} q_{D_j} P_l(\mu_{D_j})$ on both sides of Eq. (2.2) for each daughter particle and add them up. The collision term becomes

$$\sum_{l'}(-i)^{l'}(2l'+1)a^2\int\frac{đ^3\vec{q}_M}{2\epsilon_M}\prod_i\frac{đ^3\vec{q}_{Di}}{2\epsilon_{Di}}(\sum_j\epsilon_{Dj})(2\pi)^4\delta^{(4)}(\vec{q}_M-\sum_i\vec{q}_{Di}) \qquad (2.21)$$
$$\Delta f_{M(l')}P_l(\mu_{D_j})P_{l'}(\mu_M).$$

Again, our focus is on the case in which the mother particle decays after becoming non-relativistic. Then, up to corrections of order $q_M/(Ma)$ arising from the motion of the mother particle, the decay into daughters is isotropic, so that there is no correlation between the directions of the mother and daughter momenta ($\hat{n}_{M,D}$). Given that the perturbations of the daughter particles give only a small contribution to structure formation, we can ignore this subleading correction in $q_M/(Ma)$ and assume that μ_M and μ_{D_j} are uncorrelated. In this case, the angular integrals over the Legendre polynomials can be performed independently, so that

$$\sum_{l'}(-i)^{l'}(2l'+1)\int_{-1}^{1}d\mu_{D_j}P_l(\mu_{D_j})\int_{-1}^{1}d\mu_M P_{l'}(\mu_M)=0 \quad (\text{if } l \text{ or } l'>0)\,. \qquad (2.22)$$

This implies that in the daughter equations, only the zeroth moment of the source term from the mother particle decay ($\Delta f_{M(0)}$) survives in the limit of non-relativistic

decay. The source term shows up in the equation for $\Delta f'_{D(0)}$. We can therefore take $l = l' = 0$ and simplify the collision term to get a source term similar to that in Eq. (2.13), but with f^0_M replaced by the perturbation $\Delta f_{M(0)}$. Therefore, the Boltzmann hierarchy for the daughter energy perturbations, $\Delta E_{D(l)}$, in terms of the $\Delta N_{M(l)}$ and the metric perturbations h and η is given by,

$$\begin{aligned}
\Delta E'_{D(0)} &= -k\Delta E_{D(1)} - \frac{2}{3}h' E^0_D + a^2 M\Gamma \Delta N_{M(0)}, \\
\Delta E'_{D(1)} &= \frac{k}{3}\Delta E_{D(0)} - \frac{2k}{3}\Delta E_{D(2)}, \\
\Delta E'_{D(2)} &= \frac{2k}{5}\Delta E_{D(1)} - \frac{3k}{5}\Delta E_{D(3)} + \frac{4}{15}E^0_D(h' + 6\eta'), \\
\Delta E'_{D(l)} &= \frac{k}{2l+1}[l\Delta E_{D(l-1)} - (l+1)\Delta E_{D(l+1)}], \quad l \geq 3.
\end{aligned} \tag{2.23}$$

Similar equations can also be found in [72, 73, 75, 78]. Again, we neglect the source terms with $\Delta N_{M(l>0)}$ due to the additional $q_M/(Ma)$ suppressions in these terms. Other quantities such as the overdensity, perturbed pressure, energy flux/velocity-divergence, and shear stress can be calculated from these moments in the usual manner, to be fed into the perturbed Einstein field equations as detailed in [80].

2.3 Cosmological Signals of Neutrino Decay

In this section we determine the impact of decaying neutrinos on the matter power spectrum and on CMB lensing. In Sec. 2.3.1, we solve the Boltzmann equations of the previous section numerically using CLASS, and determine the matter power spectrum and the CMB lensing potential $C^{\phi\phi}_\ell$ as a function of the neutrino mass and lifetime. This

allows us to establish numerically that there is indeed a degeneracy in the matter power spectrum between neutrino mass and lifetime. In Sec. 2.3.2, we determine the matter power spectrum analytically, after making certain well-motivated approximations. We show that the results closely reproduce those based on the numerical study, and admit a physical interpretation of the effects of decaying neutrinos.

2.3.1 Numerical Results

To simplify the analysis, we assume that the three neutrinos have degenerate masses and lifetimes. This extends the parameter space of the ΛCDM model to include two additional parameters; the sum of neutrino masses, $\sum m_\nu$, and the logarithm of the decay width, $\log_{10}\Gamma_\nu$. In our analysis, we fix the following cosmological parameters to their central values from the *Planck* 2015 TT, TE, EE+low-P data:$\{\omega_b = 0.022032,\ \omega_{\rm cdm} = 0.12038,\ \ln(10^{10}A_s) = 3.052,\ n_s = 0.96229,\ \tau_{\rm reio} = 0.0648\}$. The impact of neutrino masses on the matter power spectrum looks different depending on whether θ_s or H_0 is kept fixed [68]. This is because, to keep θ_s fixed, H_0 must be adjusted within CLASS, leading to an overall shift of the matter power spectrum. While fixing H_0 is more conventional, fixing θ_s gives a better reflection of the constraining effects of a combined analysis of CMB+LSS data, since CMB data pins θ_s down very precisely. In the following, we will show results with either $H_0 = 67.56$ km/s/Mpc or $100 \times \theta_s = 1.043$, explicitly stating in each case what convention is chosen.

Since the galaxy power spectrum is known to trace the CDM and baryon overdensities,

we focus on the power spectrum

$$P_{cb}(k) = \left\langle \frac{\delta\rho_{cb}}{\bar{\rho}_{cb}} \frac{\delta\rho_{cb}}{\bar{\rho}_{cb}} \right\rangle , \tag{2.24}$$

where $\bar{\rho}_{cb}$ ($\delta\rho_{cb}$) is the average (perturbation) of the sum of CDM and baryon energy densities.[1] In Fig. 2.2, we display the residuals of P_{cb} (left) and the CMB lensing potential (right) with respect to the case of massless neutrinos for $\sum m_\nu$ fixed at 0.25 eV, keeping the value of H_0 fixed. We compare three different values of Γ_ν and the limiting case of stable neutrinos. The curves run from top to bottom in order of decreasing Γ_ν. The analytic results are shown as dashed lines in the plot, and are seen to agree reasonably well at large k or ℓ with the numerical results, shown as solid lines. These plots demonstrate that the main effect of a non-zero decay rate of neutrinos is to reduce the power suppression at large k arising from their mass. Moreover, they establish that the gravitational effects of unstable relic neutrinos can indeed give rise to observable signals in LSS, provided that the decays occur sufficiently long after the neutrinos have become non-relativistic.

Because of the effects of non-linearities at large k (small scales) and cosmic variance at small k (large scales), current experiments are sensitive only to a narrow range of k in the neighborhood of $0.1h$/Mpc. We see from Fig. 2.2 that in this region there are no qualitative features in $P_{cb}|_{z=0}$ or $C_\ell^{\phi\phi}$ that would allow unstable neutrinos to be distinguished from stable ones. Although $P_{cb}|_{z=0}$ and $C_\ell^{\phi\phi}$ are more suppressed in the stable case, as expected, this effect can be mimicked if the the neutrino masses in the unstable scenario are suitably heavier. This results in a strong parameter degeneracy

[1] Note that this is different from the matter power spectrum conventionally defined as $P_m = \langle[(\delta\rho_{cb} + \delta\rho_\nu)/(\bar{\rho}_{cb} + \bar{\rho}_\nu)]^2\rangle$, which differs from P_{cb} by an extra factor $[\bar{\rho}_{cb}/(\bar{\rho}_{cb} + \bar{\rho}_\nu)]^2$.

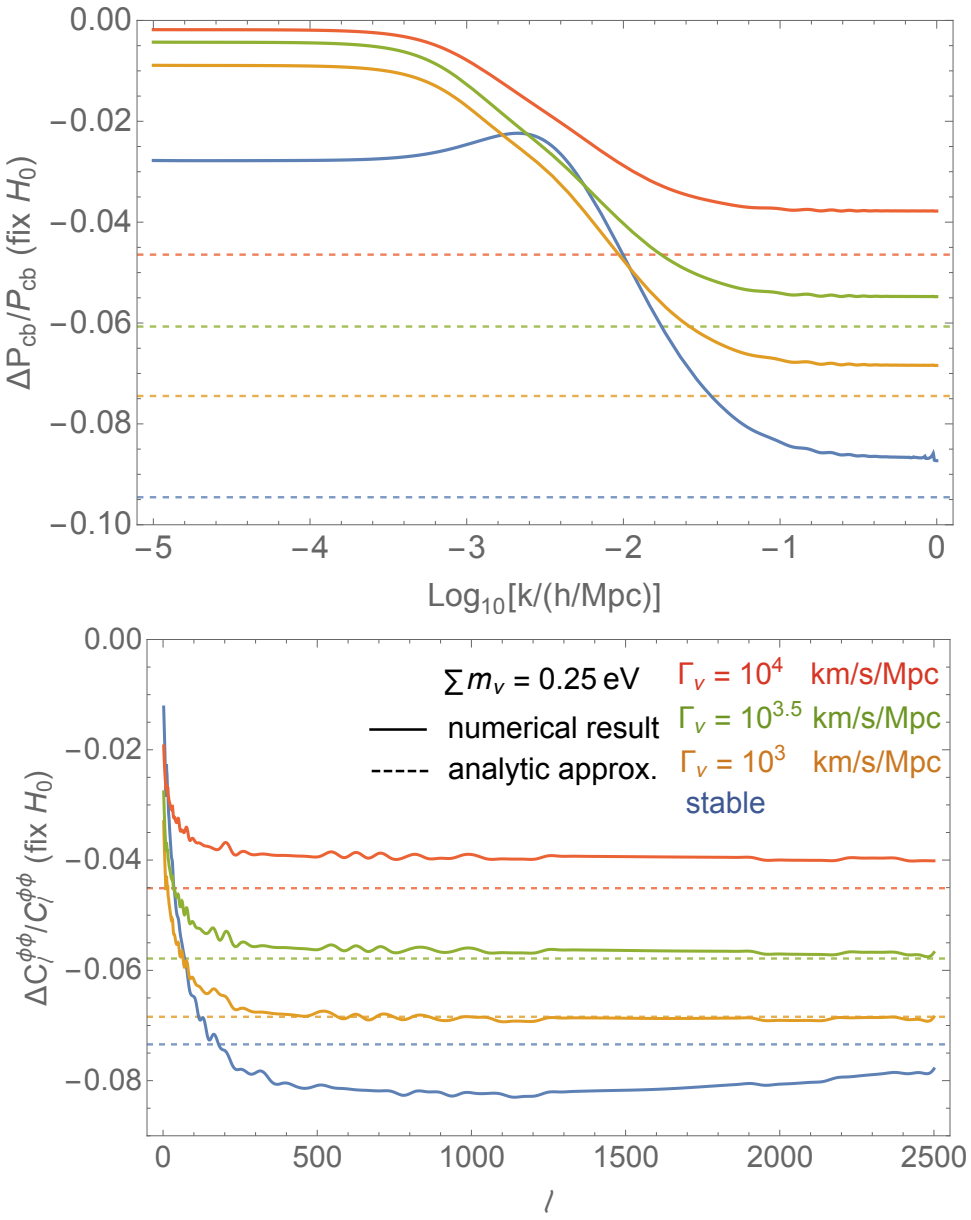

Figure 2.2: Plots of the fractional difference in the CDM+Baryon power spectrum P_{cb} (top) and CMB-lensing potential $C_\ell^{\phi\phi}$ (bottom) for various decaying (and stable) massive neutrino scenarios with respect to the case of massless neutrinos. The solid lines show the results from numerical simulations of the decaying neutrino scenario for three values of the decay width, $\Gamma_\nu = 10^{4.0,\ 3.5,\ 3.0}$ (km/s/Mpc) (top to bottom), and also the stable neutrino scenario, holding $\sum m_\nu = 0.25$ eV and H_0 fixed. The dashed lines represent the corresponding analytic estimates from Sec. 2.3.2.

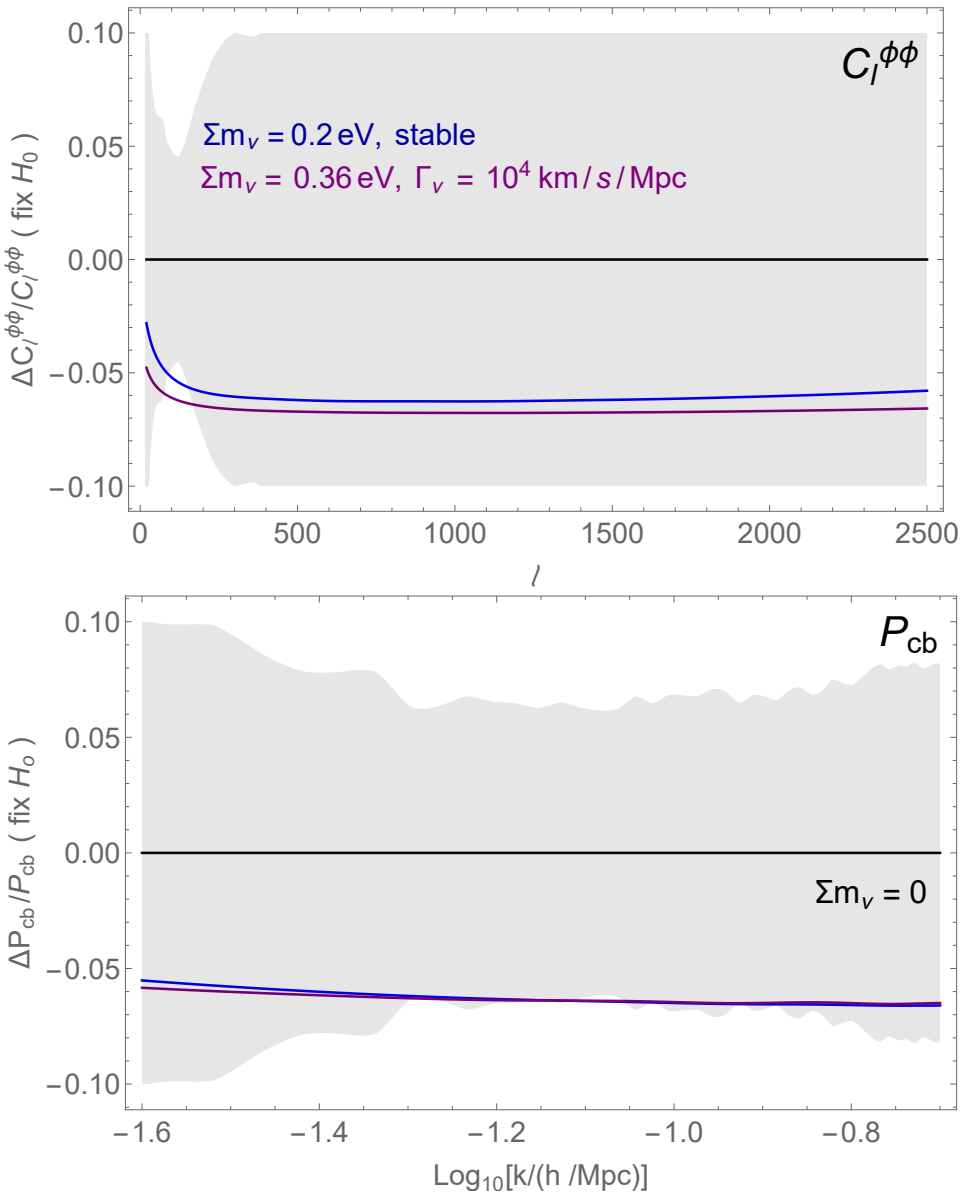

Figure 2.3: The fractional differences in the CMB-lensing potential $C_\ell^{\phi\phi}$ (top), CDM+Baryon power spectrum P_{cb} (bottom) for an unstable (purple) and a stable (blue) neutrino scenario with respect to the case of massless neutrinos (black) at fixed H_0. The grey regions show the 1σ uncertainties from *Planck* and SDSS DR7 respectively.

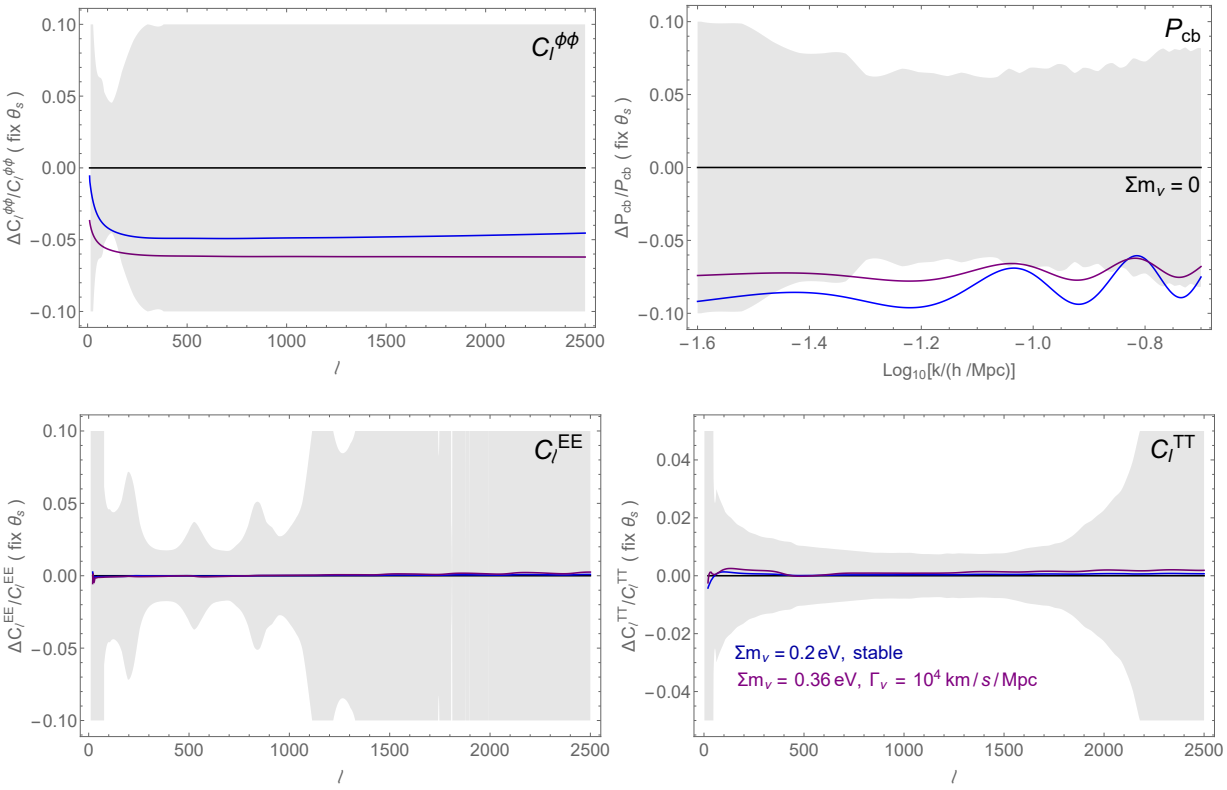

Figure 2.4: The fractional differences in the CMB-lensing potential $C_\ell^{\phi\phi}$ (top left), CDM+Baryon power spectrum P_{cb} (top right), C_ℓ^{TT} (bottom left), and C_ℓ^{EE} (bottom right) for an unstable (purple) and a stable (blue) neutrino scenario with respect to the case of massless neutrinos (black) at fixed θ_s. The grey regions show the 1σ uncertainties from *Planck* and SDSS DR7 respectively.

between the neutrino lifetime and the sum of neutrino masses as determined from $P_{cb}|_{z=0}$ and $C_\ell^{\phi\phi}$.

In Fig. 2.3 we show an explicit example of the degeneracy between mass and lifetime in the values of P_{cb} and $C_\ell^{\phi\phi}$ at fixed H_0. We consider a model with stable neutrinos of mass $\sum m_\nu = 0.2$ eV, and a different model with unstable neutrinos of mass $\sum m_\nu = 0.36$ eV and width $\Gamma_\nu = 10^4$ km/s/Mpc. In the $P_{cb}(z = 0)$ case, we see from the figure that the blue (stable neutrino) and purple (unstable neutrino) curves cannot be distinguished by measurements such as SDSS DR7 (used later in sec. 2.4), whose sensitivity is shown in grey. However, we note that the lensing power spectrum can potentially help in breaking the degeneracy, because it receives its dominant contribution at higher $z \approx 3$ [82]. We will explore the possibility of breaking the degeneracy by using next generation measurements at different redshifts in future work.

Finally, we show in Figs. 2.4 the effects of neutrino masses and decay at fixed θ_s on P_{cb}, $C_\ell^{\phi\phi}$ and $C_\ell^{TT,EE}$. This fixes the peak locations in the CMB power spectra and only generates negligible deviations away from the massless neutrino case in $C_\ell^{TT,EE}$ [68]. The same choices of parameters, however, do generate sizeable deviations in $C_\ell^{\phi\phi}$ and P_{cb} away from the massless neutrino case that are close to the current sensitivities. This demonstrates that as expected, for sub-eV $\sum m_\nu$, it is the CMB-lensing and matter power spectrum measurements that provide the constraining power. Additionally, note that the change in H_0 required to keep θ_s fixed leads to an overall shift of P_{cb}. This makes the BAO in the three models out of phase and leads to small oscillations at large k on top of the power suppression.

2.3.2 Analytic Understanding

In this section we provide an analytic derivation of the effects of neutrino decay on CMB and LSS observables. We begin by showing how the results in the literature for the effects of massive neutrinos on the matter power spectrum ($P_{cb}(k)$) and CMB lensing ($C_\ell^{\phi\phi}$) can be reproduced analytically. We improve on the existing analytical treatment of the cosmological effects of massive neutrinos by taking into account their momentum distribution. We then build on this to derive an expression for the evolution of overdensities in scenarios with unstable neutrinos.

Once neutrinos become non-relativistic, their contribution to the background energy density leads to an increase the Hubble rate, leaving less time for structure formation as compared to a universe with massless neutrinos. The net result is an overall suppression of power at small scales in the matter power spectrum. The size of this effect can be determined by studying the evolution of density perturbations. Consider $\delta_i = \delta\rho_i/\bar{\rho}_i$ for particle species i, for a mode that is already deep inside the horizon when neutrinos become non-relativistic at $z = z_{\rm nr}$. In the matter dominated era, the Einstein equation for the density perturbation with wavenumber k can be approximated as

$$k^2\phi \approx -4\pi\, G a^2(\delta_{cb}\,\bar{\rho}_{cb} + \delta_\nu\,\bar{\rho}_\nu). \tag{2.25}$$

Here ϕ is the metric perturbation in the conformal Newtonian gauge [80].[2] We assume baryons have already decoupled from photons. This allows us to combine the baryon

[2]We use the metric $ds^2 = a^2(\tau)[-(1+2\psi)d\tau^2 + (1-2\phi)\delta_{ij}dx^i dx^j]$ and approximate $\psi = -\phi$, ignoring the small correction arising from the presence of free streaming radiation.

contribution to the matter density with that of CDM to simplify the discussion. Since $\delta_\nu \ll \delta_{cb}$ for perturbation modes that enter the horizon before $z_{\rm nr}$, we can write,

$$k^2\phi \approx -\frac{6}{\tau}\left(1-\frac{\bar{\rho}_\nu(\tau)}{\bar{\rho}_{\rm tot}(\tau)}\right)\delta_{cb}, \tag{2.26}$$

where τ is the comoving time and $\bar{\rho}_{\rm tot} \equiv \bar{\rho}_{cb} + \bar{\rho}_\nu$. Inserting this expression into the Boltzmann equation for CDM perturbations yields,

$$\ddot{\delta}_{cb} + \frac{2}{\tau}\dot{\delta}_{cb} - \frac{6}{\tau^2}\left(1-f_\nu(\tau)\right)\delta_{cb} = 0, \qquad f_\nu(\tau) = \frac{\bar{\rho}_\nu(\tau)}{\bar{\rho}_{\rm tot}(\tau)}. \tag{2.27}$$

where the dots represent derivatives with respect to τ. Deep in the matter dominated era, neutrinos only contribute up to a few percent of the total energy density. Therefore, throughout this derivation, we work to leading order in f_ν ($\ll 1$). We look for a solution of the form,

$$\delta_{cb} = \delta_{cb,i}h(\tau)\left(\frac{\tau}{\tau_i}\right)^2 \exp\left[-\frac{6}{5}\int_{\tau_i}^{\tau}\frac{d\hat{\tau}}{\hat{\tau}}f_\nu(\hat{\tau})\right] \tag{2.28}$$

where now the function $h(\tau)$ is to be determined. Inserting this expression into Eq. (2.27) and dropping the term proportional to f_ν^2, we obtain the following differential equation for $h(\tau)$.

$$\tau\,\ddot{h} + 6\dot{h} - \frac{6}{5}h\,\dot{f} = 0\ . \tag{2.29}$$

Thus far we have not made any assumption about the redshift dependence of f_ν. For

massless or ultrarelativistic neutrinos in the matter dominated era, we have

$$f_\nu(\tau) = f_{\nu,i}\left(\frac{\tau_i}{\tau}\right)^2, \tag{2.30}$$

In this case we can solve for the function $h(\tau)$ as,

$$h^{\not m_\nu}(\tau) = \exp\left[k\int_{\tau_i}^{\tau} d\hat{\tau}\, \dot{f}_\nu^{\not m_\nu}(\hat{\tau})\right] = \exp\left[\frac{2}{5}\left(f_\nu^{\not m_\nu}(\tau_i) - f_\nu^{\not m_\nu}(\tau)\right)\right]. \tag{2.31}$$

This leads to the following approximate solution for perturbations in the case of massless or ultrarelativistic neutrinos,

$$\delta_{cb}^{\not m_\nu}(\tau) = \delta_{cb,i}\left(\frac{\tau}{\tau_i}\right)^2 \exp\left[-\frac{6}{5}\int_{\tau_i}^{\tau}\frac{d\hat{\tau}}{\hat{\tau}} f_\nu^{\not m_\nu}(\hat{\tau})\right]\; h^{\not m_\nu}(\tau). \tag{2.32}$$

In the limit that neutrinos are non-relativistic, $f_\nu(\tau)$ goes to a constant value. Then Eq. (2.29) admits a solution where $h(\tau)$ is constant. This implies that in the case of massive neutrinos, the h-function can be approximated as

$$h^{m_\nu}(\tau) = \exp\left\{\frac{2}{5}\left[f_\nu^{\not m_\nu}(\tau_i) - f_\nu^{\not m_\nu}\left(\min(\tau, \tau_{\rm nr})\right)\right]\right\}. \tag{2.33}$$

The result is almost identical to Eq. (2.31) since in both cases the exponent is dominated by $f_\nu^{\not m_\nu}(\tau_i)$ (and $f_\nu^{\not m_\nu}$ after $\tau > \tau_{\rm nr}$ is much smaller than the expansion parameter $f_\nu^{m_\nu}$)

$$h^{m_\nu}(\tau) \approx h^{\not m_\nu}(\tau). \tag{2.34}$$

This means that the solution in the case of massive neutrinos can be approximated as,

$$\delta_{cb}^{m_\nu}(\tau) = \delta_{cb,i}\left(\frac{\tau}{\tau_i}\right)^2 \exp\left[-\frac{6}{5}\int_{\tau_i}^{\tau}\frac{d\hat{\tau}}{\hat{\tau}} f_\nu^{m_\nu}(\hat{\tau})\right] h^{\not{m}_\nu}(\tau). \tag{2.35}$$

Then the ratio of the perturbations in the two cases is given by,

$$\frac{\delta_{cb}^{m_\nu}(\tau)}{\delta_{cb}^{\not{m}_\nu}(\tau)} = \exp\left[-\frac{6}{5}\int_{\tau_i}^{\tau}\frac{d\hat{\tau}}{\hat{\tau}}\left(f_\nu^{m_\nu}(\hat{\tau}) - f_\nu^{\not{m}_\nu}(\hat{\tau})\right)\right]. \tag{2.36}$$

This ratio can be expressed in terms of the scale factor as,

$$\frac{\delta_{cb}^{m_\nu}(a)}{\delta_{cb}^{\not{m}_\nu}(a)} \approx \frac{\delta_{cb}^{m_\nu}(a_i)}{\delta_{cb}^{\not{m}_\nu}(a_i)} \exp\left[-\frac{3}{5}\int_{a_i}^{a}\frac{da}{a}\frac{\hat{\rho}_\nu(a)}{\bar{\rho}_{\rm tot}(a)}\right], \tag{2.37}$$

where $\hat{\rho}_\nu(a) \equiv \bar{\rho}_{\nu,m_\nu}(a) - \bar{\rho}_{\nu,\not{m}_\nu}(a)$ represents the difference in the neutrino energy between the two scenarios. If all the neutrinos are stable and become non-relativistic instantly at a_i, $\hat{\rho}_\nu(a)/\bar{\rho}_{\rm tot}(a) = \bar{\rho}_{\nu,m_\nu}/\bar{\rho}_{\rm tot}$ is a constant, and Eq. (2.37) recovers the well-known result for the ratio of perturbations in the massive and massless neutrino scenarios,

$$\frac{\delta_{cb}^{m_\nu}(a)}{\delta_{cb}^{\not{m}_\nu}(a)} \propto \left(\frac{a}{a_i}\right)^{-\frac{3}{5}\frac{\bar{\rho}_{\nu,m_\nu}}{\bar{\rho}_{\rm tot}}}. \tag{2.38}$$

We can improve on this estimate by incorporating a more precise expression for the neutrino energy in Eq. (2.37),

$$\hat{\rho}_\nu(a) = 4\pi a^{-4}\int_0^\infty dq\, q^2\left(\sqrt{q^2+m_\nu^2a^2} - q\right) f(q)\ . \tag{2.39}$$

Here $q = a\,p_\nu$ denotes the neutrino's conformal momentum, and $f(q) = \left[e^{q/T_{\nu 0}} + 1\right]^{-1}$ represents the momentum distribution of neutrinos. $\hat{\rho}_\nu(a)$ exhibits non-trivial redshift dependence since the neutrino energy goes from being radiation-like to being matter-like. In fig. 2.5, we show the evolution of the ratio in Eq. (2.37) as a function of redshift (black dashed curves) for two different values of the neutrino mass. We start our approximation from $a_i = 2 \times 10^{-3}$ to make sure we are deep inside the matter dominated era so that the assumptions leading to Eq. (2.37) are justified. We stress, however, that the result is quite insensitive to $\mathcal{O}(1)$ changes in a_i. As we can see, Eq. (2.37) is a good approximation to the full numerical results (black solid curves), and describes the evolution of the δ_{cb} ratio from the relativistic to the non-relativistic regime much better than the approximation based on Eq. (2.38) (black dotted curves). Using this, we can estimate the ratio of the power spectrum between the two scenarios,

$$\frac{P_{cb,m_\nu}}{P_{cb,\not{m}_\nu}} \approx \left(\frac{\delta_{cb}^{m_\nu}(a_f)}{\delta_{cb}^{\not{m}_\nu}(a_f)}\right)^2 . \tag{2.40}$$

The density perturbation grows much slower in the cosmological constant dominant era, and we take the final scale factor to be at $a_f = 0.7$ for a good approximation to the power spectrum ratio today[3].

We now turn our attention to the effects of massive neutrinos on CMB lensing. The difference in the density perturbation $\delta\rho_{cb}$ between the massive and massless neutrino scenarios results in a change in the gravity perturbation ϕ. The photons are therefore deflected differently in the CMB lensing process. The correlation function of the lensing

[3]We can also use $a_f = a\,g(a)$ with the growth function $g(a)$ for a reasonable approximation [51].

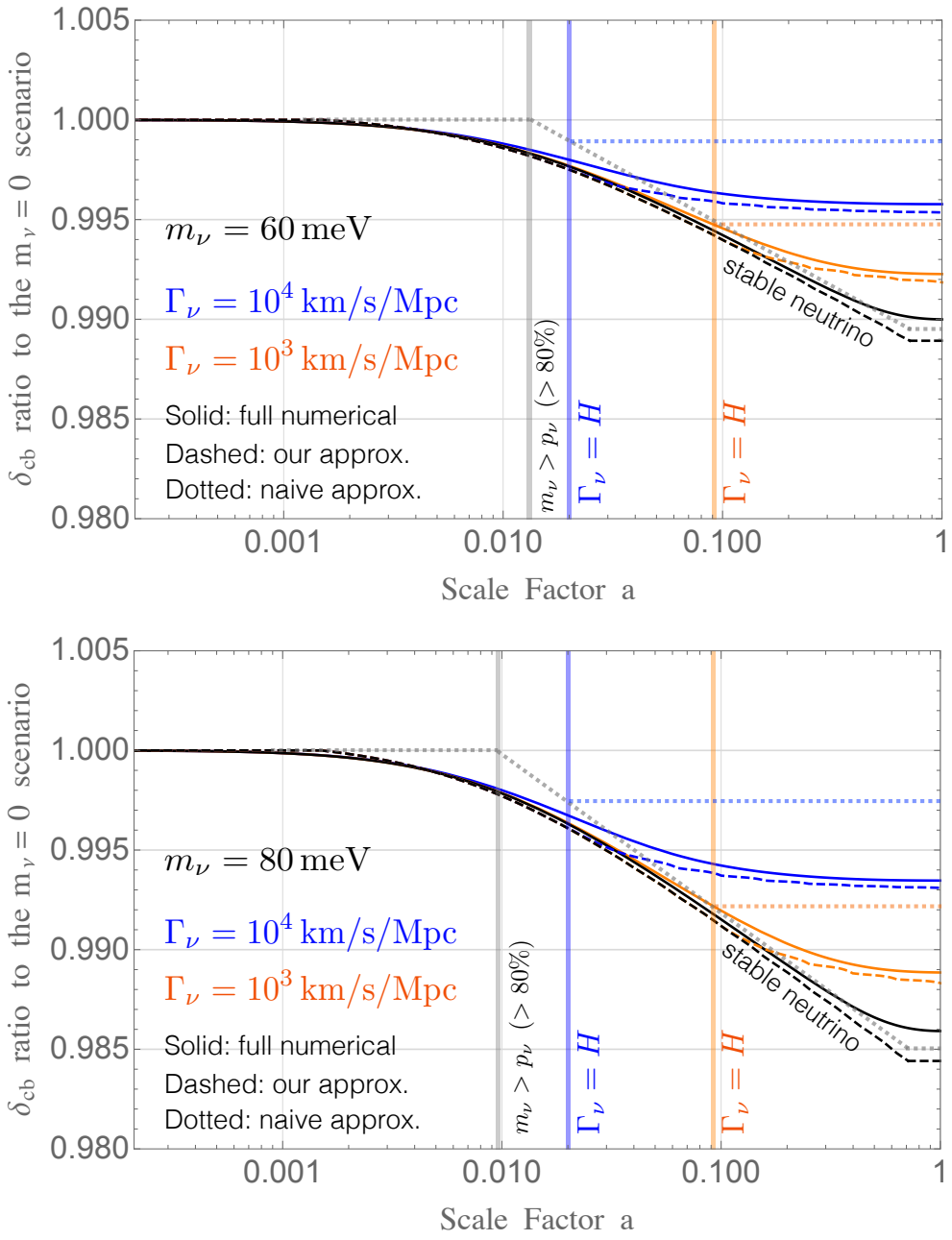

Figure 2.5: Evolution of the ratio of the CDM+baryon density perturbation with respect to the case of a massless neutrino, $\delta_{cb}^{m_\nu}/\delta_{cb}^{m_\nu=0}$. The results are shown for the case of a single massive neutrino with $m_\nu = 60$ meV. All the solid curves are obtained from numerical calculations using the modified CLASS code discussed in Sec. 2.2. The black curve is for the stable neutrino scenario, and the blue (orange) curve is for the neutrino with decay rate $\Gamma_\nu = 10^4\,(10^3)$ km/s/Mpc. The dashed curves represent the first approximations to the solid curves, based on the derivation in Eq. (2.37). The dotted curves are based on the approximation method in Eq. (2.38), where we assume a_i to be the value when 80% of neutrinos have their momenta lower than m_ν and $a_f = a_{\rm dec}$. As we see, Eq. (2.37) provides a much better approximation to the full numerical result.

potential, $C_\ell^{\phi\phi} \sim \langle\phi\phi\rangle$, parameterizes the size of angular deflection of CMB photons. The ratio of $C_\ell^{\phi\phi}$ in the massive neutrino case to that in the massless case can be approximated using Limber's formula [83, 84]

$$\frac{C^{\phi\phi}_{\ell,\,m_\nu}}{C^{\phi\phi}_{\ell,\not{m}_\nu}} \approx \frac{\chi_*^{m_\nu}\displaystyle\int_0^1 \mathrm{d}x\,\phi^2_{m_\nu}\left(\frac{\ell}{x^{m_\nu}\chi_*}\right)(1-x)^2}{\chi_*^{\not{m}_\nu}\displaystyle\int_0^1 \mathrm{d}x\,\phi^2_{\not{m}_\nu}\left(\frac{\ell}{x^{\not{m}_\nu}\chi_*}\right)(1-x)^2}\,, \quad x \equiv \frac{\tau_f-\tau}{\tau_f-\tau_*}\,, \quad \chi_* \equiv \tau_f - \tau_*\,. \tag{2.41}$$

Here $\tau_* \approx 2.8\times10^2$ Mpc is the conformal time at last scattering, while $\tau_f \approx 1.4\times10^4$ Mpc is the conformal time today. The value of τ_f differs a bit between the massive and massless neutrino scenarios, since the contribution of neutrinos to the total energy density is different in the two cases. However, since the neutrino mass only results in a significant difference in the contributions to the background energy in the short period of time between the neutrinos becoming non-relativistic and the universe becoming dominated by the cosmological constant, the difference in χ_* between the two scenarios can be neglected. Then, the difference between $C_\ell^{\phi\phi}$ in the two cases primarily arises from differences in the evolution of ϕ.

According to the Einstein Eq. (2.25), the ratio of ϕ between the two scenarios for large ℓ modes at a given value of the scale factor is,

$$\frac{\phi_{m_\nu}(a)}{\phi_{\not{m}_\nu}(a)} \approx \frac{\delta_{cb}^{m_\nu}(a)}{\delta_{cb}^{\not{m}_\nu}(a)}\,. \tag{2.42}$$

Since $C_\ell^{\phi\phi}$ receives its dominant contribution close to $z \approx 3$ [82], we can estimate the

ratio of the $C_\ell^{\phi\phi}$ as,

$$\frac{C^{\phi\phi}_{\ell,\,m_\nu}}{C^{\phi\phi}_{\ell,\not{m}_\nu}} \approx \left(\frac{\delta^{m_\nu}_{cb}}{\delta^{\not{m}_\nu}_{cb}}\right)^2 \Bigg|_{z=3} . \tag{2.43}$$

Based on a very similar analysis, we can predict the suppression of $P_{cb}(k)$ and $C_\ell^{\phi\phi}$ for large k and ℓ in the unstable neutrino case. We consider a scenario with a single massive neutrino species that becomes non-relativistic after last scattering and decays into dark radiation. After the decay, the energy density of the *daughter* particles redshifts more quickly than that of a stable neutrino of the same mass as the mother. We work in the instantaneous decay approximation and assume that all neutrinos decay at the same time, corresponding to a scale factor $a_{\rm dec}$, which is implicitly determined by the equation,

$$\Gamma_\nu = H(a_{\rm dec}). \tag{2.44}$$

The difference in energy density $\hat{\rho}_\nu$ between an unstable neutrino and a massless neutrino evolves in a more complicated way than in the case of a stable neutrino. The instantaneous decay approximation allows us to separate the evolution into two parts. On timescales shorter than the proper lifetime of the neutrino, the difference in energy density follows the equation,

$$\hat{\rho}_\nu(a) = 4\pi a^{-4}\int_0^\infty dq\, q^2 \left(\sqrt{q^2+m_\nu^2 a^2} - q\right) f(q)\,, \quad a < a_{\rm dec}\,. \tag{2.45}$$

In the instantaneous decay approximation, the energy density in non-relativistic neutrinos is immediately transferred into radiation energy at $a_{\rm dec}$. It subsequently redshifts with an

extra $(a_{\rm dec}/a)$ factor as compared to a non-relativistic neutrino, so that

$$\hat{\rho}_\nu(a) = 4\pi a^{-4} \int_0^\infty dq\, q^2 \left[\sqrt{q^2 + m_\nu^2 a^2}\left(\frac{a_{\rm dec}}{a}\right) - q\right] f(q)\,, \quad a \geq a_{\rm dec}\,. \tag{2.46}$$

The ratio of CDM density perturbations in the case of unstable neutrinos can be obtained by inserting the energy density ratios in Eqs. (2.45) and (2.46) into Eq. (2.37). Then the ratios of $P(k)$ and $C_\ell^{\phi\phi}$ in the limit of large k and ℓ can be obtained from Eqs. (2.40) and (2.43)

In Fig. 2.5, we show the ratio of δ_{cb} from the numerical calculation described in Sec. 2.2 for both the decaying (blue and orange) and stable (black) neutrinos. The plots are for a single massive neutrino with $m_\nu = 60$ meV (upper) and 80 meV (lower), and a decay rate $\Gamma_\nu = 10^4\,(10^3)$ km/s/Mpc for the blue (orange) curves. In this scenario, more than 80% of the neutrinos have momenta $p_\nu < m_\nu$ after $a > 0.012$ ($a > 0.0096$) for $m_\nu = 60\,(80)$ meV neutrino. It is at this point, when most of the neutrinos have become non-relativistic, that the major suppression of δ_{cb} begins. During this period the δ_{cb} ratio drops with the power described in Eq. (2.38) (grey line). The blue (orange) dotted lines give the value of the δ_{cb}-suppression if the later contributions of daughter particles to the energy density shown in Eq. (2.46) are ignored. As we see, this underestimates the suppression of δ_{cb}, showing that the contributions of daughter particles to the energy density cannot be neglected. It is clear from the figures that Eqs. (2.45) and (2.46) provide a good description of the δ_{cb} evolution in unstable neutrino scenarios (dashed blue and orange), both before and after neutrino decay. This shows that the effects of neutrino decay on the evolution of δ_{cb} on these length scales primarily arise from the contributions

of the unstable neutrinos and their daughter particles to the background energy density, and not from their perturbations.

2.4 Current Limits on the Neutrino Mass and Lifetime from Monte Carlo Analysis

In this section we perform a Monte Carlo analysis to determine the current bounds on the neutrino mass and lifetime.

2.4.1 The Data and Analysis Pipeline

Our analysis makes use of various combinations of the following datasets.

- CMB: We include *Planck* 2015 CMB high-ℓ TT, TE, and EE and low-ℓ TEB power spectra [85], as well as the lensing reconstruction power spectrum [86].
- BAO: We use measurements of the volume distance from 6dFGS at $z = 0.106$ [87] and the MGS galaxy sample of SDSS at $z = 0.15$ [88]. We include the anisotropic measurements from the CMASS and LOWZ galaxy samples from the BOSS DR12 at $z = 0.38$, 0.51, and 0.61 [89].
- Growth Function: The BOSS DR12 measurements also include measurements of the growth function f, defined by

$$f\sigma_8 \equiv \frac{\left[\sigma_8^{(vd)}(z)\right]^2}{\sigma_8^{(dd)}(z)}\,, \tag{2.47}$$

where $\sigma_8^{(vd)}$ measures the smoothed density-velocity correlation, analogous to $\sigma_8 \equiv \sigma_8^{(dd)}$ that measures the smoothed density-density correlation.

- Pantheon: we use the Pantheon supernovae dataset [90], which includes measurements of the luminosity distance of 1048 SNe Ia in the redshift range $0.01 < z < 2.3$.

- LSS: We use the measurement of the halo power spectrum from the Luminous Red Galaxies SDSS-DR7 [91][4] and the tomographic weak lensing power spectrum by KiDS [92].

Our baseline analysis makes use of Planck+BAO+Growth Function+Pantheon data (i.e. data that relies on background cosmology or perturbations in the linear regime mostly). We then add LSS information to gauge the constraining power of such surveys.

Using the public code MONTEPYTHON-V3[5] [93, 94], we run Monte Carlo Markov chain analyses using the Metropolis-Hastings algorithm assuming flat priors on all parameters. Our ΛCDM parameters are, $\{\omega_{\rm cdm}, \omega_b, \theta_s, \ln(10^{10} A_s), n_s, \tau_{\rm reio}\}$, to which we add the sum of neutrino masses $\sum m_\nu$ and the logarithm of the neutrino lifetime $\mathrm{Log}_{10}\Gamma_\nu$. In our analysis we assume 3 degenerate, unstable neutrino species that decay into dark radiation. Although not detailed for brevity, there are many nuisance parameters that we analyze together with these cosmological parameters. To that end, we employ a Cholesky decomposition to handle the large number of nuisance parameters [95], and use the default priors that are provided by MONTEPYTHON-V3.

[4] More recent measurements are not yet available in MONTEPYTHON-V3. These could naturally make the bounds presented here slightly stronger.

[5] https://github.com/brinckmann/montepython_public

2.4.2 Current Limits on the Neutrino Mass and Lifetime

In order to perform meaningful comparisons and to check the accuracy of our modified version of CLASS, we begin by running the case of *stable* neutrinos. Our baseline constraint on the neutrino mass, obtained with Planck+BAO+Growth Function+Pantheon, is $\sum m_\nu < 0.28$ eV (95% C.L.). This is in good agreement with the result reported in [61]. The inclusion of SDSS DR7 and KiDS improves the constraint by $\sim 10\%$, bringing the limit down to $\sum m_\nu < 0.25$ eV (95% C.L.). This constraint when LSS data is included is also in good agreement with what is reported in Ref. [96].

In Fig. 2.6 we show the 1D and 2D marginalized posterior distribution of $\sum m_\nu$ and $\log_{10}\Gamma_\nu$ for both datasets, cutting the parameter space between small decay rate $\log_{10}\Gamma_\nu/(\mathrm{km/s/Mpc}) \in [0, 3]$ (left panel) and large decay rate $\log_{10}\Gamma_\nu/(\mathrm{km/s/Mpc}) \in [3, 5.5]$ (right panel) to accelerate convergence. Strikingly, once the neutrino lifetime is let free to vary, the constraint on $\sum m_\nu$ is driven by our prior on $\log_{10}\Gamma_\nu$. We recall that this was chosen in order to ensure that neutrinos decay while non-relativistic. Interestingly, the constraint stays quite stable for $\log_{10}\Gamma_\nu/(\mathrm{km/s/Mpc}) < 2.5$, but relaxes to $\sum m_\nu < 0.9$ eV (with Planck+BAO+Growth Function+Pantheon) for higher values of the decay rate. We note that the limit only marginally improves with the addition of current LSS data, especially at high decay rates (right panel), for which the improvement is below numerical noise.

Our study allows us to obtain a bound on the sum of neutrino masses as a function of the neutrino lifetime. We see that $\sum m_\nu$ can be as large as 0.90 eV for neutrinos that decay close to recombination. However, given our restricted prior enforcing non-

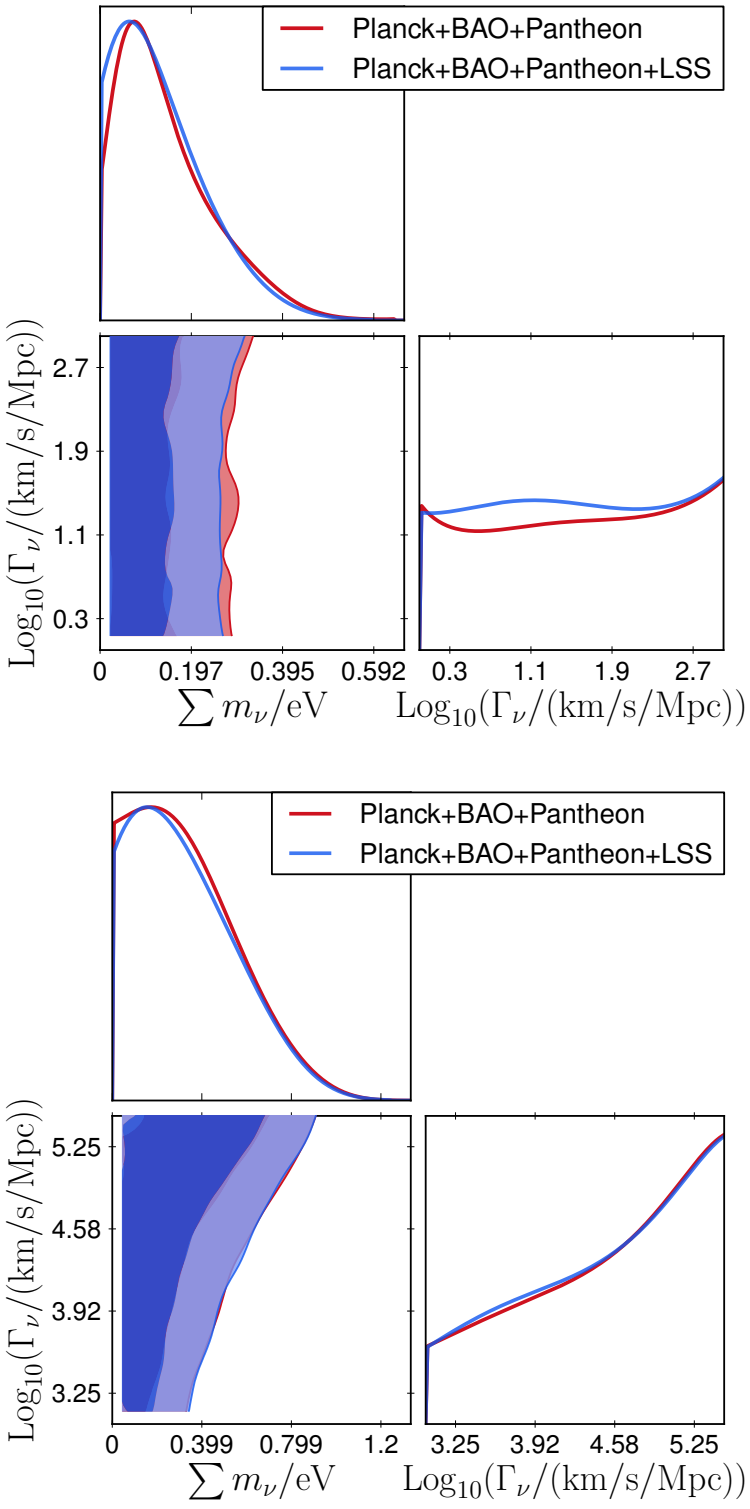

Figure 2.6: Posterior distributions of $\sum m_\nu$ and $\log_{10}\Gamma_\nu$ for each dataset. Small decay rate $\log_{10}\Gamma_\nu/(\mathrm{km/s/Mpc}) \in [0, 3]$ are shown in the top panel, while large decay rate $\log_{10}\Gamma_\nu/(\mathrm{km/s/Mpc}) \in [3, 5.5]$ are shown in the bottom panel.

relativistic decays, our analysis does not set a true upper bound on the neutrino mass. In order to derive the true upper bound we would need to correctly incorporate relativistic decays, taking into account inverse decay processes. A nice discussion of this regime with inverse decays is given in Ref. [35, 38] for the interested reader. In the light of the latest *Planck* results, a reanalysis of this regime will be very interesting.

Chapter 3: Measuring Neutrino Lifetime from LSS Tomography

3.1 Lifting the Degeneracy Between Neutrino Mass and Lifetime

In the last chapter, we saw that the sensitivity of cosmological observables to the neutrino masses arises from the fact that, after the neutrinos become non-relativistic, their contribution to the energy density redshifts like matter, and is therefore greater than that of a relativistic species of the same abundance. This leads to a faster Hubble expansion, reducing the time available for structure formation. The net result is an overall suppression of large scale structure [48, 49], (for reviews see [50, 51, 52, 53]). A larger neutrino mass gives rise to greater suppression, since heavier neutrinos become non-relativistic at earlier times, and also contribute more to the total energy density after becoming non-relativistic. In the case of neutrinos that decay, the extent of the suppression now also depends on the neutrino lifetime. The key idea, first discussed in [54, 55], is that if the neutrinos decay into massless species after becoming non-relativistic, the suppression in power is reduced. Depending on how late the decay kicks in after the neutrinos have become non-relativistic, the magnitude of the suppression will vary.

These features are illustrated in Fig. 3.1, where we show the evolution of the overdensity of cold dark matter and baryons, $\delta_{cb} \equiv \delta\rho_{cb}/\bar{\rho}_{cb}$, for three cases, based on the analysis

Table 3.1: Forecast constraints on the sum of neutrino masses (at 68% C.L.) and decay width of the heaviest neutrino (at 95% C.L.) from Fig. 3.2

Normal ordering					
Fiducial $\sum m_\nu$/eV	0.06	0.12	0.18	0.24	0.30
$\sum m_\nu$/eV	< 0.085	$0.125^{+0.020}_{-0.020}$	$0.183^{+0.017}_{-0.017}$	$0.243^{+0.016}_{-0.016}$	$0.303^{+0.015}_{-0.015}$
$\mathrm{Log}_{10}\left[\frac{\Gamma_\nu}{\mathrm{km/s/Mpc}}\right]$	< 3.7	< 3.2	< 2.1	< 1.7	< 1.5
Inverted ordering					
Fiducial $\sum m_\nu$/eV	0.10	0.15	0.20	0.25	0.30
$\sum m_\nu$/eV	< 0.13	$0.154^{+0.017}_{-0.017}$	$0.205^{+0.015}_{-0.017}$	$0.253^{+0.016}_{-0.016}$	$0.304^{+0.015}_{-0.015}$
$\mathrm{Log}_{10}\left[\frac{\Gamma_\nu}{\mathrm{km/s/Mpc}}\right]$	< 2.7	< 2.2	< 1.8	< 1.5	< 1.3

in [59] and briefly described in the next section. The results are expressed in terms of the ratio of $(\delta_{cb})^2$ for each case to its value in the scenario with massless neutrinos. The black line corresponds to stable neutrinos with $\sum m_\nu = 0.25$ eV, while the blue line corresponds to unstable neutrinos of the same mass. To simplify the discussion, in this plot we have taken the lifetimes Γ_ν of all the three neutrinos to be the same. We see that, as compared to the stable neutrino scenario, unstable neutrinos of the same mass lead to a smaller suppression of δ_{cb} at $z = 0$. The red line corresponds to unstable neutrinos with $\sum m_\nu = 0.30$ eV, and their lifetime has been chosen to obtain the same result for the overdensity at $z = 0$ as for stable neutrinos with $\sum m_\nu = 0.25$ eV. We see from the black and red curves in Fig. 3.1 that the effects of a stable neutrino on the matter density perturbations cannot be easily distinguished from those of a heavier neutrino that is shorter-lived based only on measurements performed at $z \lesssim 0.3$. This is because the growth of δ_{cb} is almost frozen in the region where the cosmological constant dominates ($z \lesssim 0.3$). Therefore, there is a degeneracy between $\sum m_\nu$ and τ_ν that cannot be resolved based only on measurements of the matter power spectrum at low redshifts. However, it is

clear from Fig. 3.1 that the evolution of the power suppression at earlier times is different in the two cases. Consequently, the shapes of the power spectra as a function of z are distinct. This would allow these two cases to be distinguished if measurements are made at more than one redshift with sub-percent precision (e.g., black vs. red at $z = 0.5$ and $z = 2$ in Fig. 3.1).

The near future Euclid experiment is expected to take measurements at multiple redshifts between $z \approx 0.5$ and $z \approx 2$ at very high level of precision. Hence the combined Euclid and Planck data has the potential to break the degeneracy between neutrino mass and lifetime.

3.2 Prospects of Measuring Neutrino Lifetime from Near-future Euclid and CMB-S4 Experiments

In order to calculate the effects of neutrino decay on cosmological observables, we implement the Boltzmann equations corresponding to the decay of neutrinos into dark radiation that were derived in [59] into the code CLASS [60]. We work under the assumption that, after becoming non-relativistic, each SM neutrino decays with width Γ_{ν_i} into two massless particles. Here the indices i label the neutrino mass eigenstates. For concreteness, we assume that the decay widths of the three neutrinos satisfy the relation $\Gamma_{\nu_i} \propto m_{\nu_i}^3$. This assumption is motivated by models in which the generation of neutrino masses is associated with the breaking of global symmetries. Since Goldstone bosons are derivatively coupled, in these theories the matrix element for neutrino decay typically scale as m_ν/f, where f corresponds to the scale at which the global symmetry is broken.

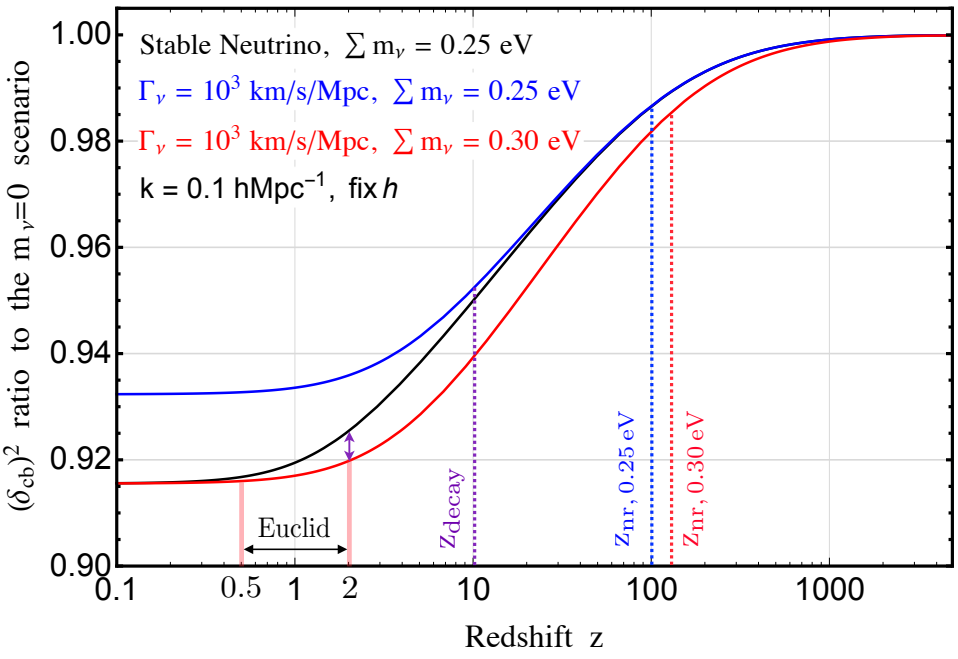

Figure 3.1: Evolution of the ratio of the CDM+baryon density perturbations with respect to the case of massless neutrinos. The blue (black) curve corresponds to the case of stable (unstable) massive neutrinos with $\sum m_\nu = 0.25$ eV. Here $z_{\rm decay}$, defined as the redshift at which the neutrino width Γ_ν becomes equal to the Hubble constant, corresponds to the redshift at the time of neutrino decay. Similarly $z_{\rm nr}$ denotes the redshift at which 80% of the neutrinos have become non-relativistic. Unstable heavier neutrinos with $\sum m_\nu = 0.3$ eV (red) can give the same density perturbation at low redshift as stable neutrinos of mass $\sum m_\nu = 0.25$ eV. However, at $z = 2$, the perturbation in the heavier neutrino scenario deviates at the $\mathcal{O}(0.1)\%$ level from the stable neutrino scenario (purple arrow).

Then, after accounting for phase space, we typically have $\Gamma_{\nu_i} \sim m_{\nu_i}^3$. Given the observed mass splittings, this leaves only two remaining independent parameters. We choose to present the results of our analysis in terms of the parameters $(\sum m_\nu, \Gamma_\nu)$, where Γ_ν is the decay width of the heaviest neutrino. With this definition, $\Gamma_\nu \equiv \Gamma_{\nu_3}$ for the normal ordering and $\Gamma_\nu \equiv \Gamma_{\nu_2}$ for the inverted ordering. For the same values of $\sum m_\nu$ and Γ_ν, the results for the normal and inverted ordering are different. This is because the individual neutrino masses are different in the two cases. Therefore the neutrinos become non-relativistic at different times and have different lifetimes. These differences become

increasingly small for values of $\sum m_\nu$ above 0.2 eV, since in this regime the neutrinos are quasi-degenerate.

Table 3.2: Forecast constraints at 68% C.L. on the sum of neutrino masses and decay width of the heaviest neutrino from Fig 3.3.

Fiducial $(\mathrm{Log}_{10}\left[\frac{\Gamma_\nu}{\mathrm{km/s/Mpc}}\right], \sum m_\nu/\mathrm{eV})$	$(3.7, 0.16)$	$(3, 0.25)$
$\sum m_\nu/\mathrm{eV}$	$0.167^{+0.035}_{-0.076}$	$0.261^{+0.042}_{-0.069}$
$\mathrm{Log}_{10}\left[\frac{\Gamma_\nu}{\mathrm{km/s/Mpc}}\right]$	$3.59^{+0.65}_{-0.45}$	$2.96^{+0.64}_{-0.46}$
$\sum m_\nu/\mathrm{eV}$ (stable)	$0.10^{+0.02}_{-0.02}$	$0.19^{+0.02}_{-0.02}$

We wish to determine the extent to which a combination of Planck data and future Euclid data can help break the degeneracy between the neutrino mass and lifetime. To that end, we make use of the mock likelihoods available publicly in MONTEPYTHON-V3.1 and described in Refs. [94, 97]. We include Euclid galaxy and cosmic shear power spectra in the "realistic" configuration, i.e., we include nonlinear scales and employ a loose (redshift-independent) non-linear cut at comoving $k_{\rm NL} = 2\ h/\mathrm{Mpc}$ in the galaxy power spectrum and $k_{\rm NL} = 10\ h/\mathrm{Mpc}$ in the cosmic shear power spectrum, together with a nonlinear correction based on HaloFit [98, 99] and a theoretical error on the nonlinear modeling (as described in Refs. [94, 97]). For a few cases, we employed an alternative "conservative" prescription where we cut the data at comoving $k_{\rm NL} = 0.2\ h/\mathrm{Mpc}$ in the galaxy power spectrum and $k_{\rm NL} = 0.5\ h/\mathrm{Mpc}$ in the cosmic shear power spectrum, and verified that this leads to very similar results. This gives us confidence in the robustness of our conclusions. In order to include Planck data in our forecast, we generate a mock dataset with the fake likelihood FAKE_PLANCK_REALISTIC available in MONTEPYTHON-V3.1. We analyze chains using the python package GETDIST [100].

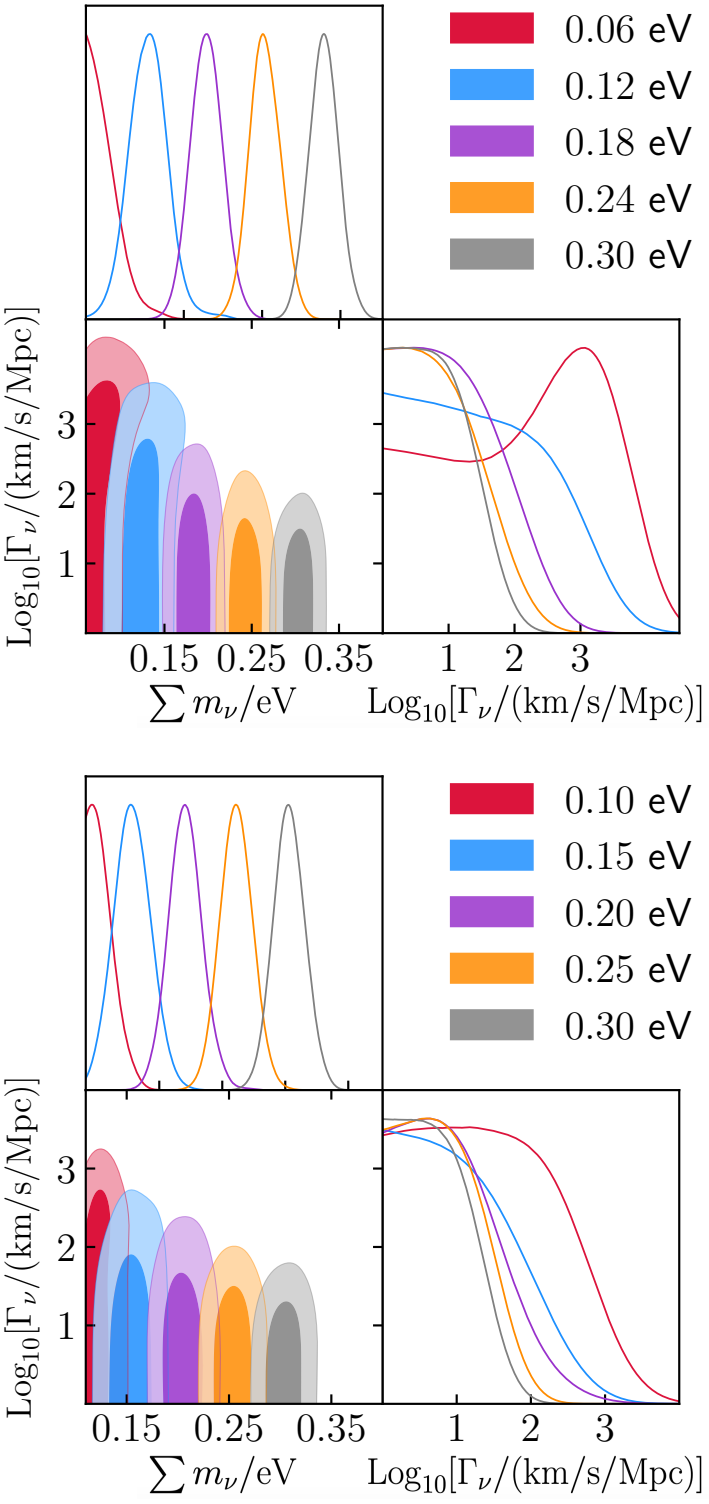

Figure 3.2: Forecast of the 2D posterior of the sum of neutrino masses (at 68% C.L.) and decay width of the heaviest neutrino (at 95% C.L.) reconstructed from a combination of Planck+Euclid $P(k)$+Euclid Lensing. The fiducial model assumes that neutrinos are stable and that they follow the normal ordering (top panel) or inverted ordering (bottom panel).

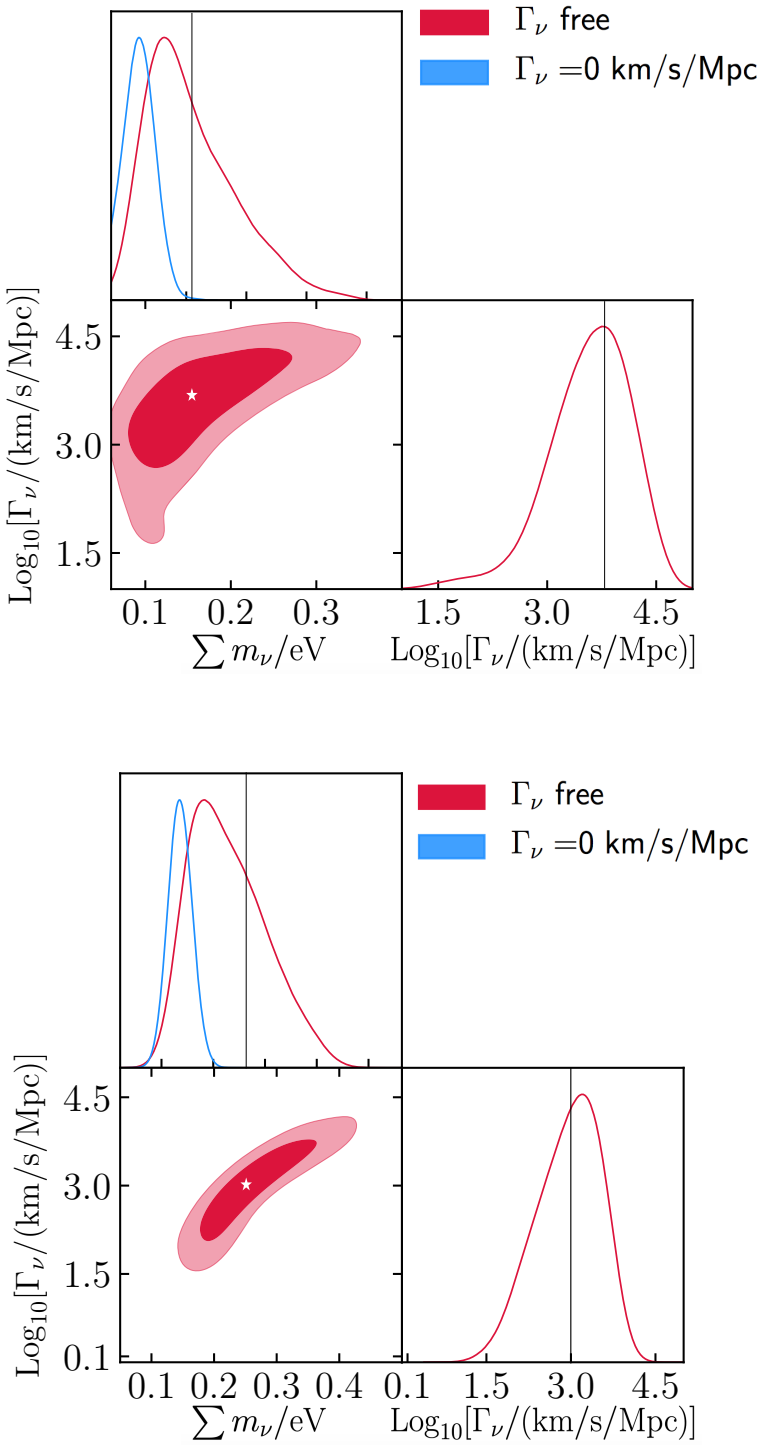

Figure 3.3: Same as Fig. 3.2, but the fiducial model now assumes decaying neutrinos with $(\mathrm{Log}_{10}[\Gamma_\nu/(\mathrm{km/s/Mpc})], \sum m_\nu/\mathrm{eV}) = (3.7, 0.16)$ (top panel) and $(3, 0.25)$ (bottom panel) in the normal ordering. The stars and dashed lines indicate the fiducial values of the corresponding parameters.

We first forecast the lower bound on the neutrino lifetime that can be reached in the near future. We begin by generating mock data sets for the case of stable neutrinos, i.e., $\Gamma_\nu = 0$. Specifically, we generate a mock data set for the following values of $\sum m_\nu$/eV: $[0.06, 0.12, 0.18, 0.24, 0.30]$ for the case of normal ordering and $[0.10, 0.15, 0.20, 0.25, 0.30]$ for inverted ordering. This range covers the minimum $\sum m_\nu$ allowed by the normal and inverted mass spectra, and also the maximum $\sum m_\nu$ consistent with the current bound derived in [59]. We then run one MCMC scan per mock data set varying the ΛCDM parameters $\{\omega_b, \omega_{\rm cdm}, 100\theta_s, A_s, n_s, \tau_{\rm reio}\}$ together with $\{\sum m_\nu/{\rm eV}, {\rm Log}_{10}[\Gamma_\nu/({\rm km/s/Mpc})]\}$. As mentioned earlier, here Γ_ν refers to the width of the heaviest neutrino. As our modifications to CLASS have the effect of making the code much slower, we are forced to run a large number of chains (~ 100) to acquire enough points to obtain robust results. This penalizes the use of the Gelman-Rubin criterion [101] as a convergence test. Nevertheless, all runs satisfy the Gelman-Rubin criterion except for the cases with fiducial $\sum m_\nu/{\rm eV} = 0.06$, $\sum m_\nu/{\rm eV} = 0.10$ and $\sum m_\nu/{\rm eV} = 0.12$. For these runs, we have at most $(R-1) \approx 0.3$, $(R-1) \approx 0.22$ and $(R-1) \approx 0.25$ respectively. Therefore we primarily rely on visual inspections, and on comparison between various chunks of chains, to assess convergence. As a check, we have verified that for all scenarios, our constraints vary by less than 10% when adapting the fraction of points removed with GETDIST from 0.1 to 0.5.

Our results are displayed in Fig. 3.2 for the normal- (top) and inverted- (bottom) mass ordering cases, where we show the bounds on the decay rate Γ_ν of the heaviest neutrino as a function of $\sum m_\nu$. We summarize the bounds on the neutrino masses and lifetime for both hierarchies in Table 3.1. Of utmost importance, we find that the combination of Planck and Euclid can break the degeneracy between $(\sum m_\nu, \Gamma_\nu)$ and

set an upper bound on the neutrino lifetime, $\mathrm{Log}_{10}[\Gamma_\nu/(\mathrm{km/s/Mpc})] \leq 3.7$ (2σ), even for the lowest possible neutrino mass. Moreover, we find that the sensitivity to $\sum m_\nu$ is not significantly degraded by the additional free parameter $\log_{10}\Gamma_\nu$. As can be seen from Table 3.1, the bounds on Γ_ν in the normal and inverted ordering cases become increasingly close above $\sum m_\nu \gtrsim 0.2$ eV. This is because in this limit the neutrinos are becoming quasi-degenerate. Nevertheless, even for $\sum m_\nu = 0.3$ eV, the values of the two largest neutrino masses differ at the level of a few percent between the normal and inverted hierarchies. Since $\Gamma_\nu \propto m_\nu^3$, this accounts for the $\sim 10\%$ difference between the bounds on Γ_ν in the two cases. Finally, we mention that we do not find any strong correlation between the decay rate and the other cosmological parameters. Therefore, for brevity we do not explicitly report the reconstructed ΛCDM parameters.

Given these constraints on $\mathrm{Log}_{10}[\Gamma_\nu/(\mathrm{km/s/Mpc})]$, we anticipate that future cosmological data will be able to determine that neutrinos are decaying if the width exceeds this limit. To demonstrate this, we turn our attention to a scenario with unstable neutrinos and generate two sets of mock data corresponding to $(\mathrm{Log}_{10}[\Gamma_\nu/(\mathrm{km/s/Mpc})], \sum m_\nu/\mathrm{eV}) = (3.7, 0.16)$ and $(3, 0.25)$ with a normal ordering. For each mock data set and fiducial model we run two cases, one in which we leave Γ_ν free to vary and another in which we enforce the constraint $\Gamma_\nu = 0$. The purpose of the latter case is to allow us to estimate the typical bias that would be introduced if this scenario was actually realized in nature and neutrino decays were not accounted for. The results of both these runs satisfy the Gelman-Rubin criterion.

Our results are shown in Fig. 3.3 and summarized in Table 3.2. We find, as expected, that for both cases the combination of Planck and Euclid sets an upper limit on the

neutrino lifetime, so that the decaying neutrino scenario can be distinguished from the stable case at better than 3σ. Remarkably, in both cases we also obtain a lower limit on the neutrino lifetime at 3σ, opening the door to the possibility of determining the neutrino lifetime from cosmology.

Based on our limits, one might expect that the neutrino lifetime can be determined at better than 2σ provided $\mathrm{Log}_{10}[\Gamma_\nu/(\mathrm{km/s/Mpc})] > 3.7$ for $\sum m_\nu/\mathrm{eV} > 0.06$. However, recall that the regime $\mathrm{Log}_{10}[\Gamma_\nu/(\mathrm{km/s/Mpc})] \gtrsim 5$ is not treated in our formalism, since neutrinos would be decaying while still relativistic. We defer a detailed study of the parameter space for which next-generation experiments can determine the neutrino lifetime to future work.

Interestingly, we find that in both the cases considered, the precision at which $\sum m_\nu$ can be detected is strongly degraded compared to the contours in Fig. 3.2. Indeed, in these cases the uncertainty on $\sum m_\nu$ is multiplied by ~ 5 when Γ is let free to vary, and ~ 1.5 when $\Gamma_\nu = 0$ is enforced. This is of great importance for next-generation experiments which claim that a combination of datasets will be able to detect the sum of neutrino masses "at 5σ", even in the minimal mass case. Perhaps even more important, we find that when $\Gamma_\nu = 0$ is enforced, a strong bias in the reconstructed neutrino mass away from the true value can appear. For the specific cases studied here, we find a bias of roughly -0.06 eV, i.e, a $\sim 3\sigma$ shift away from the "true" value.

Chapter 4: Conclusion

The fact that the couplings of neutrinos to the other SM particles are so weak makes it extremely difficult to study their properties. Even though it has been over six decades since neutrinos were first directly observed in the laboratory, several of their fundamental properties, including their masses and lifetimes, remain to be determined. However, neutrinos are also among the most abundant particles in the universe, and their gravitational pull has effects on cosmological observables. The universe is therefore an excellent laboratory for studying the detailed properties of neutrinos.

In this dissertation, we have explored the cosmological signals arising from the theoretically well-motivated scenario in which massive neutrinos decay into invisible dark radiation on timescales less than the age of the universe. We have studied the effects of neutrino decay on the evolution of density perturbations, both analytically and numerically, and used these results to generalize the bound on the sum of neutrino mass to the case when the lifetime of the neutrino is less than the age of the universe. Our analytical results show that the signals of neutrino decay in LSS and CMB-lensing primarily arise from the contributions of neutrinos and their daughters to the overall energy density, and are quite insensitive to their contributions to the fluctuations about the background. We find that the effect of increasing the neutrino-mass on CMB and LSS

can be compensated by decreasing the lifetime. This leads to a parameter degeneracy between the neutrino mass and neutrino lifetime inferred from the cosmological data.

Due to this parameter degeneracy, we show that the existing mass bound from CMB and LSS measurements, which assumes that neutrinos are stable, gets weakened if neutrinos decay, so that values of $\sum m_\nu$ as large as 0.9 eV are still allowed by the data. This provides strong motivation to continue the current efforts to measure the neutrino masses directly in the lab, in spite of the limited reach of these experiments.

While the existing LSS data do not set independent constraints on the neutrino mass and lifetime, we show that the next generation measurements of the matter power spectrum at different redshifts can break this degeneracy and allow us to determine the sum of neutrino masses and the neutrino lifetime independently. We find that near-future measurements by the Euclid satellite can improve the lower limit on the neutrino lifetime in this scenario from $\mathcal{O}(10)$ years to 200 million years. In the case of neutrinos that decay on shorter timescales these measurements may allow the neutrino lifetime to be determined from cosmology.

In our analysis we have focused on the decay of neutrinos to dark radiation, which is easier to distinguish from the case of stable neutrinos than the decay of heavier neutrinos to lighter ones. However, we expect that our results also give a good approximation to the latter scenario in the limit that the lightest neutrino is massless. This applies to both the normal and inverted hierarchies, and shows that future observations will have some level of sensitivity to this interesting class of theories.

Appendix A: A Model of Massive Neutrino Decay into Dark Radiation

In this appendix we present a simple, realistic model in which massive neutrinos decay into invisible dark radiation on timescales of order the age of the universe. To illustrate the main features of the model, we first consider a simplified version with just a single flavor of SM neutrino, denoted by ν, and two singlet right-handed neutrinos, labelled as n and n'. The model also contains two complex scalars, labelled as Φ and Φ'. We introduce $U(1)_n \times U(1)_{n'}$ global symmetries that act on the right-handed neutrinos. While n and Φ carry equal and opposite charges under $U(1)_n$, n' and Φ' are neutral under this symmetry. Similarly, n' and Φ' carry equal and opposite charges under $U(1)_{n'}$, while n and Φ are neutral. Then the part of the Lagrangian responsible for generating the neutrino masses takes the form,

$$-\mathcal{L} \supset \frac{y}{\Lambda}\bar{L}\tilde{H}n\Phi + \frac{y'}{\Lambda}\bar{L}\tilde{H}n'\Phi' + \text{H.c.} \tag{A.1}$$

Here L represents the SM lepton doublet and $\tilde{H} = i\sigma_2 H^*$, where H denotes the SM Higgs doublet. Λ is a UV mass scale while y and y' are coupling constants. Although this Lagrangian is nonrenormalizable, it can be interpreted as the low energy description of a renormalizable theory after particles with masses of Λ have been integrated out. For

example, consider the renormalizable Lagrangian,

$$-\mathcal{L} = \tilde{y}\bar{L}\tilde{H}N + M_N N N^C + \tilde{\lambda} n N^c \Phi + \tilde{y}'\bar{L}\tilde{H}N' + M'_N N' N^{c\prime} + \tilde{\lambda}' n' N^{c\prime}\Phi' + \text{H.c.} \quad \text{(A.2)}$$

Terms of the form shown in Eqn. (A.1) are obtained after the heavy fermions N, N^c N' and $N^{c\prime}$ have been integrated out.

Once the scalars Φ, Φ' and the SM Higgs each acquire a vacuum expectation value (VEV), we obtain Dirac masses for the SM neutrino,

$$-\mathcal{L} \supset \frac{yfv}{2\Lambda}\bar{\nu}n + \frac{y'f'v}{2\Lambda}\bar{\nu}n' + \text{H.c.} = m\bar{\nu}n_{\text{h}} + \text{H.c.}. \quad \text{(A.3)}$$

Here $\frac{f}{\sqrt{2}}$, $\frac{f'}{\sqrt{2}}$ and $\frac{v}{\sqrt{2}}$ denote the VEVs of Φ, Φ' and H respectively. The SM neutrino acquires a mass $m = \sqrt{(yf)^2 + (y'f')^2}v/(2\Lambda)$. Its Dirac partner n_{h} is one linear combination of n and n',

$$\begin{pmatrix} n_{\text{h}} \\ n_{\text{l}} \end{pmatrix} = \begin{pmatrix} \cos\theta & \sin\theta \\ -\sin\theta & \cos\theta \end{pmatrix} \begin{pmatrix} n \\ n' \end{pmatrix} \; ; \; \cos\theta = \frac{yf}{\sqrt{(yf)^2 + (y'f')^2}}. \quad \text{(A.4)}$$

It is clear from Eq. (A.3) that the spectrum contains one massive Dirac neutrino and one massless singlet neutrino n_{l}.

Below the spontaneous symmetry breaking scales f and f', the Goldstone bosons can be parametrized as

$$\Phi = \frac{f}{\sqrt{2}}e^{i\phi/f} \quad , \quad \Phi' = \frac{f'}{\sqrt{2}}e^{i\phi'/f'}, \quad \text{(A.5)}$$

where ϕ and ϕ' denote the Goldstone bosons from $U(1)_n$ and $U(1)_{n'}$ respectively. The couplings of the Goldstone bosons in the low energy effective theory are dictated by the non-linearly realized global symmetries. To leading order in $1/f$ and $1/f'$, they are given by,

$$-\mathcal{L} \supset i\frac{yfv}{2\Lambda}\frac{\phi}{f}\bar{\nu}n + i\frac{yf'v}{2\Lambda}\frac{\phi'}{f'}\bar{\nu}n + \text{H.c.} \tag{A.6}$$

In the mass basis these interactions take the form,

$$-\mathcal{L} \supset im\bar{\nu}\left[\left(\frac{\phi}{f}\cos^2\theta + \frac{\phi'}{f'}\sin^2\theta\right)n_{\text{h}} + \left(\frac{\phi'}{f'} - \frac{\phi}{f}\right)\sin\theta\cos\theta\, n_{\text{l}}\right] + \text{H.c.} \tag{A.7}$$

We see from this that the massive neutrino can decay into n_{l} and either ϕ or ϕ'. Its partial widths into these decay modes are given by,

$$\Gamma(\nu \to n_{\text{l}}\phi) = \frac{m^3}{32\pi\bar{f}^2}\ ,\ \Gamma(\nu \to n_{\text{l}}\phi') = \frac{m^3}{32\pi\bar{f}'^2}, \tag{A.8}$$

where $\bar{f} \equiv f/(\cos\theta\sin\theta)$ and $\bar{f}' \equiv f'/(\cos\theta\sin\theta)$.

Now we move on to discuss the realistic case in which there are three flavors of SM neutrinos ν_α ($\alpha = e\,,\mu\,,\tau$). We also introduce three flavors of the sterile neutrinos n_α and n'_α, as well as a new scalar field $\Sigma_{\alpha\beta}$. The global symmetry in the neutrino sector is now extended to $SU(3)_L \times SU(3)_R \times U(1)_n \times U(1)_{n'}$. The charge assignments under $U(1)_n \times U(1)_{n'}$ are the same as before, but with all 3 flavors of n_α and n'_α now being charged under $U(1)_n$ and $U(1)_{n'}$ respectively. Under $SU(3)_L \times SU(3)_R$, the various

fields transform as

$$L \to U_L\, L \qquad n \to U_R\, n \qquad n' \to U_R\, n' \qquad \Sigma \to U_L \Sigma U_R^\dagger\,, \tag{A.9}$$

where U_L and U_R are the rotation matrices of $SU(3)_L$ and $SU(3)_R$ respectively. The neutrino masses now arise from terms in the Lagrangian of the form,

$$-\mathcal{L} \supset \frac{y}{\Lambda^2}\bar{L}_\alpha \tilde{H} \Sigma_{\alpha\beta} n_\beta \Phi + \frac{y'}{\Lambda^2}\bar{L}_\alpha \tilde{H} \Sigma_{\alpha\beta} n'_\beta \Phi' + \text{H.c.} \tag{A.10}$$

Once the Σ field acquires a VEV, we can diagonalize its VEV $\langle\Sigma\rangle$ to obtain,

$$-\mathcal{L} \supset \sum_i \left(\frac{y}{\Lambda^2}\bar{L}_i \tilde{H} \langle\Sigma\rangle_i n_i \Phi + \frac{y'}{\Lambda^2}\bar{L}_i \tilde{H} \langle\Sigma\rangle_i n'_i \Phi' \right) + \text{H.c.} \tag{A.11}$$

where the index i runs over $i = 1, 2, 3$ and $\langle\Sigma\rangle_i$ denotes the ith eigenvalue of $\langle\Sigma\rangle$. The Lagrangian in Eq. (A.11) can be viewed as three copies of Eq. (A.1). After the scalars Φ, Φ' and H acquire VEVs, all three generations of $(n_i\,, n'_i)$ can be simultaneously transformed to the mass basis $(n_{\mathrm{h}i}, n_{\mathrm{l}i})$ using the same orthogonal matrix,

$$\begin{pmatrix} n_{\mathrm{h}i} \\ \\ n_{\mathrm{l}i} \end{pmatrix} = \begin{pmatrix} \cos\theta & \sin\theta \\ \\ -\sin\theta & \cos\theta \end{pmatrix} \begin{pmatrix} n_i \\ \\ n'_i \end{pmatrix}, \tag{A.12}$$

where $\cos\theta$ is exactly the same as in Eq. (A.4). Now the neutrino masses are given by,

$$m_i = \sqrt{(yf)^2 + (y'f')^2}\,\frac{\langle\Sigma\rangle_i v}{2\Lambda^2}. \tag{A.13}$$

Assuming that the Goldstone bosons from Σ are heavier than the massive neutrinos due to some external source of explicit breaking, the dominant decay modes of the massive neutrinos are to a massless sterile neutrino and either ϕ or ϕ'. Following the discussion above, the total neutrino decay width is given by

$$\Gamma_{\nu_i} = \Gamma(\nu_i \to n_{1_i}\phi) + \Gamma(\nu_i \to n_{1_i}\phi') = \frac{m_i^3}{32\pi \bar{f}^2} + \frac{m_i^3}{32\pi \bar{f}'^2}, \tag{A.14}$$

where $\bar{f}$ and $\bar{f}'$ are as defined after Eq. (A.8). One characteristic feature of this model is that the widths of the neutrinos scale as the cube of their masses, $\Gamma_{\nu_i}/\Gamma_{\nu_j} = m_i^3/m_j^3$. In the case of quasi-degenerate neutrinos, $m_1 \approx m_2 \approx m_3$, it is clear that all neutrinos have almost the same total width. Assuming $\bar{f} = \bar{f}'$, we find that the total width is of order H_0 for $\bar{f} \sim 10^5$ and neutrino masses of order 0.1 eV,

$$\frac{\Gamma_{\nu_i}}{H_0} \approx 1.3 \left(\frac{m_i}{0.1 \text{ eV}}\right)^3 \left(\frac{10^5}{\bar{f}}\right)^2. \tag{A.15}$$

The parameter space of this model is constrained by astrophysical, cosmological and laboratory data. These limits are very similar to those on conventional Majoron models, and can be expressed in terms of bounds on the decay constants f and f'. In the case of massless Goldstone bosons, the bounds from cosmology and astrophysics are the most severe. A strong cosmological constraint arises from requiring consistency with the observation that the cosmic neutrinos are free streaming at temperatures below an eV [35, 36, 37, 38]. Neutrino-neutrino scattering mediated by Goldstone boson exchange can prevent the neutrinos from free streaming, impacting the heights and locations of

the CMB peaks. This translates into constraints on f and f' of order 100 keV [102]. A stronger although somewhat model-dependent constraint, $f, f' \gtrsim 100$ MeV, may be obtained by requiring that the Goldstone bosons and right-handed neutrinos not contribute significantly to the energy density in radiation at the time of Big Bang nucleosynthesis (BBN), or during the CMB epoch.

The strongest astrophysical bounds arise from the effects of Goldstone bosons on supernovae. The large chemical potential for electron neutrinos inside the supernova means that these particles can now decay into final states containing a Goldstone boson and a right-handed neutrino. This has the effect of deleptonizing the core, preventing the explosion from taking place. In addition, the free streaming of Goldstone bosons out of the supernovae core can lead to overly rapid energy loss. The resulting constraints are at the level of $f, f' \gtrsim 100$ keV [103, 104, 105, 106, 107]. There are also bounds on the couplings of neutrinos to Goldstone bosons from laboratory experiments, such as neutrinoless double beta decay [108, 109], meson decays [103, 110], charged lepton decays [111] and tritium decay [112]. These constraints arise from corrections to the energy spectrum of the visible final states due to Goldstone boson emission. However, in all these cases, the limits are weaker than astrophysical and cosmological bounds on massless Goldstone bosons. Clearly, our benchmark values of $f, f' \sim 10^5$ GeV are easily consistent with all current bounds.

Bibliography

[1] P. F. de Salas, D. V. Forero, S. Gariazzo, P. Martínez-Miravé, O. Mena, C. A. Ternes, M. Tórtola, and J. W. F. Valle. 2020 global reassessment of the neutrino oscillation picture. *JHEP*, 02:071, 2021.

[2] S. T. Petcov. The Processes mu $\rightarrow$ e Gamma, mu $\rightarrow$ e e anti-e, Neutrino' $\rightarrow$ Neutrino gamma in the Weinberg-Salam Model with Neutrino Mixing. *Sov. J. Nucl. Phys.*, 25:340, 1977. [Erratum: Yad. Fiz.25,1336(1977)].

[3] J.Terrance Goldman and Jr. Stephenson, G.J. Limits on the Mass of the Muon-neutrino in the Absence of Muon Lepton Number Conservation. *Phys. Rev. D*, 16:2256, 1977.

[4] W. J. Marciano and A. I. Sanda. Exotic Decays of the Muon and Heavy Leptons in Gauge Theories. *Phys. Lett.*, 67B:303–305, 1977.

[5] Benjamin W. Lee and Robert E. Shrock. Natural Suppression of Symmetry Violation in Gauge Theories: Muon - Lepton and Electron Lepton Number Nonconservation. *Phys. Rev.*, D16:1444, 1977.

[6] Palash B. Pal and Lincoln Wolfenstein. Radiative Decays of Massive Neutrinos. *Phys. Rev.*, D25:766, 1982.

[7] R. N. Mohapatra and P. B. Pal. Massive neutrinos in physics and astrophysics. *World Sci. Lect. Notes Phys.*, 41:1–318, 1991.

[8] F. Boehm and P. Vogel. *Physics of Massive Neutrinos*. June 1992.

[9] G. B. Gelmini and M. Roncadelli. Left-Handed Neutrino Mass Scale and Spontaneously Broken Lepton Number. *Phys. Lett.*, 99B:411–415, 1981.

[10] Y. Chikashige, R.N. Mohapatra, and R.D. Peccei. Are there real goldstone bosons associated with broken lepton number? *Physics Letters B*, 98(4):265–268, Jan 1981.

[11] Howard M. Georgi, Sheldon Lee Glashow, and Shmuel Nussinov. Unconventional Model of Neutrino Masses. *Nucl. Phys.*, B193:297–316, 1981.

[12] J.W.F. Valle. Fast neutrino decay in horizontal majoron models. *Physics Letters B*, 131(1):87 – 90, 1983.

[13] G. B. Gelmini and J. W. F. Valle. Fast Invisible Neutrino Decays. *Phys. Lett.*, 142B:181–187, 1984.

[14] Gia Dvali and Lena Funcke. Small neutrino masses from gravitational θ-term. *Phys. Rev.*, D93(11):113002, 2016.

[15] Lena Funcke, Georg Raffelt, and Edoardo Vitagliano. Distinguishing Dirac and Majorana neutrinos by their decays via Nambu-Goldstone bosons in the gravitational-anomaly model of neutrino masses. *Phys. Rev. D*, 101(1):015025, 2020.

[16] John N. Bahcall, N. Cabibbo, and A. Yahil. Are neutrinos stable particles? *Phys. Rev. Lett.*, 28:316–318, 1972. [,285(1972)].

[17] Z. G. Berezhiani, G. Fiorentini, M. Moretti, and Anna Rossi. Fast neutrino decay and solar neutrino detectors. *Z. Phys.*, C54:581–586, 1992.

[18] A. Acker, S. Pakvasa, and James T. Pantaleone. Decaying Dirac neutrinos. *Phys. Rev. D*, 45:1–4, 1992.

[19] Vernon D. Barger, J. G. Learned, S. Pakvasa, and Thomas J. Weiler. Neutrino decay as an explanation of atmospheric neutrino observations. *Phys. Rev. Lett.*, 82:2640–2643, 1999.

[20] Andy Acker and Sandip Pakvasa. Solar neutrino decay. *Phys. Lett.*, B320:320–322, 1994.

[21] Sandhya Choubey, Srubabati Goswami, and Debasish Majumdar. Status of the neutrino decay solution to the solar neutrino problem. *Physics Letters B*, 484(1):73 – 78, 2000.

[22] Anjan S. Joshipura, Eduard Masso, and Subhendra Mohanty. Constraints on decay plus oscillation solutions of the solar neutrino problem. *Phys. Rev.*, D66:113008, 2002.

[23] A. G. Doroshkevich and M. Yu. Khlopov. Formation of structure in a universe with unstable neutrinos. *Monthly Notices of the Royal Astronomical Society*, 211(2):277–282, 11 1984.

[24] A. G. Doroshkevich, A. A. Klyin, and M. Yu. Khlopov. Cosmological models with unstable neutrinos. *Soviet Astronomy*, 32(2):127–133, 3 1988.

[25] Marco Chianese, Pasquale Di Bari, Kareem Farrag, and Rome Samanta. Probing relic neutrino radiative decays with 21 cm cosmology. *Phys. Lett.*, B790:64–70, 2019.

[26] Jelle L. Aalberts et al. Precision constraints on radiative neutrino decay with CMB spectral distortion. *Phys. Rev.*, D98:023001, 2018.

[27] A. G. Beda, V. B. Brudanin, V. G. Egorov, D. V. Medvedev, V. S. Pogosov, E. A. Shevchik, M. V. Shirchenko, A. S. Starostin, and I. V. Zhitnikov. Gemma experiment: The results of neutrino magnetic moment search. *Phys. Part. Nucl. Lett.*, 10:139–143, 2013.

[28] M. Agostini et al. Limiting neutrino magnetic moments with Borexino Phase-II solar neutrino data. *Phys. Rev.*, D96(9):091103, 2017.

[29] G. G. Raffelt. New bound on neutrino dipole moments from globular cluster stars. *Phys. Rev. Lett.*, 64:2856–2858, 1990.

[30] G. G. Raffelt. Limits on neutrino electromagnetic properties: An update. *Phys. Rept.*, 320:319–327, 1999.

[31] S. Arceo-Díaz, K. P. Schröder, K. Zuber, and D. Jack. Constraint on the magnetic dipole moment of neutrinos by the tip-RGB luminosity in ω-Centauri. *Astropart. Phys.*, 70:1–11, 2015.

[32] P. J. E. Peebles. The Role of Neutrinos in the Evolution of Primeval Adiabatic Perturbations. *Astrophys. J.*, 180:1, 1973.

[33] Wayne Hu and Naoshi Sugiyama. Small scale cosmological perturbations: An Analytic approach. *Astrophys. J.*, 471:542–570, 1996.

[34] Sergei Bashinsky and Uros Seljak. Neutrino perturbations in CMB anisotropy and matter clustering. *Phys.Rev.*, D69:083002, 2004.

[35] Maria Archidiacono and Steen Hannestad. Updated constraints on non-standard neutrino interactions from Planck. *JCAP*, 1407:046, 2014.

[36] Benjamin Audren et al. Robustness of cosmic neutrino background detection in the cosmic microwave background. *JCAP*, 1503:036, 2015.

[37] Brent Follin, Lloyd Knox, Marius Millea, and Zhen Pan. First Detection of the Acoustic Oscillation Phase Shift Expected from the Cosmic Neutrino Background. *Phys. Rev. Lett.*, 115(9):091301, 2015.

[38] Miguel Escudero and Malcolm Fairbairn. Cosmological Constraints on Invisible Neutrino Decays Revisited. *Phys. Rev. D*, 100(10):103531, 2019.

[39] Christina D. Kreisch, Francis-Yan Cyr-Racine, and Olivier Doré. The Neutrino Puzzle: Anomalies, Interactions, and Cosmological Tensions. 2019.

[40] Joshua A. Frieman, Howard E. Haber, and Katherine Freese. Neutrino Mixing, Decays and Supernova Sn1987a. *Phys. Lett.*, B200:115–121, 1988.

[41] John F. Beacom and Nicole F. Bell. Do solar neutrinos decay? *Phys. Rev.*, D65:113009, 2002.

[42] Abhijit Bandyopadhyay, Sandhya Choubey, and Srubabati Goswami. Neutrino decay confronts the SNO data. *Phys. Lett.*, B555:33–42, 2003.

[43] M. C. Gonzalez-Garcia and M. Maltoni. Status of Oscillation plus Decay of Atmospheric and Long-Baseline Neutrinos. *Phys. Lett.*, B663:405–409, 2008.

[44] R. A. Gomes, A. L. G. Gomes, and O. L. G. Peres. Constraints on neutrino decay lifetime using long-baseline charged and neutral current data. *Phys. Lett.*, B740:345–352, 2015.

[45] Sandhya Choubey, Debajyoti Dutta, and Dipyaman Pramanik. Invisible neutrino decay in the light of NOvA and T2K data. *JHEP*, 08:141, 2018.

[46] B. Aharmim et al. Constraints on Neutrino Lifetime from the Sudbury Neutrino Observatory. *Phys. Rev.*, D99(3):032013, 2019.

[47] N. Aghanim et al. Planck 2018 results. VI. Cosmological parameters. 2018.

[48] J. R. Bond, G. Efstathiou, and J. Silk. Massive Neutrinos and the Large Scale Structure of the Universe. *Phys. Rev. Lett.*, 45:1980–1984, 1980. [,61(1980)].

[49] Wayne Hu, Daniel J. Eisenstein, and Max Tegmark. Weighing neutrinos with galaxy surveys. *Phys. Rev. Lett.*, 80:5255–5258, 1998.

[50] Yvonne Y. Y. Wong. Neutrino mass in cosmology: status and prospects. *Ann. Rev. Nucl. Part. Sci.*, 61:69–98, 2011.

[51] Julien Lesgourgues, Gianpiero Mangano, Gennaro Miele, and Sergio Pastor. *Neutrino Cosmology*. Cambridge University Press, 2018.

[52] M Tanabashi et al. Review of Particle Physics. *Phys. Rev. D*, 98(3):030001. 1898 p, 2018.

[53] Massimiliano Lattanzi and Martina Gerbino. Status of neutrino properties and future prospects - Cosmological and astrophysical constraints. *Front.in Phys.*, 5:70, 2018.

[54] Pasquale D. Serpico. Cosmological neutrino mass detection: The best probe of neutrino lifetime. *Phys. Rev. Lett.*, 98:171301, 2007.

[55] Pasquale D. Serpico. Neutrinos and cosmology: a lifetime relationship. *J. Phys. Conf. Ser.*, 173:012018, 2009.

[56] John F. Beacom, Nicole F. Bell, and Scott Dodelson. Neutrinoless universe. *Phys. Rev. Lett.*, 93:121302, 2004.

[57] Yasaman Farzan and Steen Hannestad. Neutrinos secretly converting to lighter particles to please both KATRIN and the cosmos. *JCAP*, 1602(02):058, 2016.

[58] Zackaria Chacko, Abhish Dev, Peizhi Du, Vivian Poulin, and Yuhsin Tsai. Determining the Neutrino Lifetime from Cosmology. *Phys. Rev. D*, 103(4):043519, 2021.

[59] Zackaria Chacko, Abhish Dev, Peizhi Du, Vivian Poulin, and Yuhsin Tsai. Cosmological Limits on the Neutrino Mass and Lifetime. *JHEP*, 04:020, 2020.

[60] Diego Blas, Julien Lesgourgues, and Thomas Tram. The Cosmic Linear Anisotropy Solving System (CLASS) II: Approximation schemes. *JCAP*, 1107:034, 2011.

[61] P. A. R. Ade et al. Planck 2015 results. XIII. Cosmological parameters. *Astron. Astrophys.*, 594:A13, 2016.

[62] J. Angrik et al. KATRIN design report 2004. 2005.

[63] A. Gando et al. Search for Majorana Neutrinos near the Inverted Mass Hierarchy Region with KamLAND-Zen. *Phys. Rev. Lett.*, 117(8):082503, 2016. [Addendum: Phys. Rev. Lett.117,no.10,109903(2016)].

[64] M. Auger et al. The EXO-200 detector, part I: Detector design and construction. *JINST*, 7:P05010, 2012.

[65] J. B. Albert et al. Search for Majorana neutrinos with the first two years of EXO-200 data. *Nature*, 510:229–234, 2014.

[66] Luca Amendola et al. Cosmology and fundamental physics with the Euclid satellite. *Living Rev. Rel.*, 16:6, 2013.

[67] Kevork N. Abazajian et al. CMB-S4 Science Book, First Edition. 2016.

[68] Maria Archidiacono, Thejs Brinckmann, Julien Lesgourgues, and Vivian Poulin. Physical effects involved in the measurements of neutrino masses with future cosmological data. *JCAP*, 1702(02):052, 2017.

[69] Thejs Brinckmann, Deanna C. Hooper, Maria Archidiacono, Julien Lesgourgues, and Tim Sprenger. The promising future of a robust cosmological neutrino mass measurement. *JCAP*, 1901:059, 2019.

[70] M. Tanabashi et al. Review of Particle Physics. *Phys. Rev.*, D98(3):030001, 2018.

[71] Thomas Brunner and Lindley Winslow. Searching for $0\nu\beta\beta$ decay in ^{136}Xe – towards the tonne-scale and beyond. *Nucl. Phys. News*, 27(3):14–19, 2017.

[72] Benjamin Audren, Julien Lesgourgues, Gianpiero Mangano, Pasquale Dario Serpico, and Thomas Tram. Strongest model-independent bound on the lifetime of Dark Matter. *JCAP*, 1412(12):028, 2014.

[73] Vivian Poulin, Pasquale D. Serpico, and Julien Lesgourgues. A fresh look at linear cosmological constraints on a decaying dark matter component. *JCAP*, 1608(08):036, 2016.

[74] M. Kawasaki, Gary Steigman, and Ho-Shik Kang. Cosmological evolution of an early decaying particle. *Nucl. Phys.*, B403:671–706, 1993.

[75] Somnath Bharadwaj and Shiv K. Sethi. Decaying neutrinos and large scale structure formation. *Astrophys. J. Suppl.*, 114:37, 1998.

[76] Manoj Kaplinghat, Robert E. Lopez, Scott Dodelson, and Robert J. Scherrer. Improved treatment of cosmic microwave background fluctuations induced by a late decaying massive neutrino. *Phys. Rev.*, D60:123508, 1999.

[77] Shohei Aoyama, Kiyotomo Ichiki, Daisuke Nitta, and Naoshi Sugiyama. Formulation and constraints on decaying dark matter with finite mass daughter particles. *JCAP*, 1109:025, 2011.

[78] Mei-Yu Wang and Andrew R. Zentner. Effects of Unstable Dark Matter on Large-Scale Structure and Constraints from Future Surveys. *Phys. Rev.*, D85:043514, 2012.

[79] Shohei Aoyama, Toyokazu Sekiguchi, Kiyotomo Ichiki, and Naoshi Sugiyama. Evolution of perturbations and cosmological constraints in decaying dark matter models with arbitrary decay mass products. *JCAP*, 1407:021, 2014.

[80] Chung-Pei Ma and Edmund Bertschinger. Cosmological perturbation theory in the synchronous and conformal Newtonian gauges. *Astrophys. J.*, 455:7–25, 1995.

[81] Julien Lesgourgues and Thomas Tram. Fast and accurate CMB computations in non-flat FLRW universes. *JCAP*, 1409(09):032, 2014.

[82] F. Bernardeau. Weak lensing detection in CMB maps. *Astron. Astrophys.*, 324:15–26, 1997.

[83] D. N. Limber. The Analysis of Counts of the Extragalactic Nebulae in Terms of a Fluctuating Density Field. *ApJ*, 117:134, January 1953.

[84] Z. Pan, L. Knox, and M. White. Dependence of the Cosmic Microwave Background Lensing Power Spectrum on the Matter Density. *Mon. Not. Roy. Astron. Soc.*, 445(3):2941–2945, 2014.

[85] N. Aghanim et al. Planck 2015 results. XI. CMB power spectra, likelihoods, and robustness of parameters. *Astron. Astrophys.*, 594:A11, 2016.

[86] P. A. R. Ade et al. Planck 2015 results. XV. Gravitational lensing. *Astron. Astrophys.*, 594:A15, 2016.

[87] Florian Beutler, Chris Blake, Matthew Colless, D. Heath Jones, Lister Staveley-Smith, Lachlan Campbell, Quentin Parker, Will Saunders, and Fred Watson. The 6dF Galaxy Survey: Baryon Acoustic Oscillations and the Local Hubble Constant. *Mon. Not. Roy. Astron. Soc.*, 416:3017–3032, 2011.

[88] Ashley J. Ross, Lado Samushia, Cullan Howlett, Will J. Percival, Angela Burden, and Marc Manera. The clustering of the SDSS DR7 main Galaxy sample – I. A 4 per cent distance measure at $z = 0.15$. *Mon. Not. Roy. Astron. Soc.*, 449(1):835–847, 2015.

[89] Shadab Alam et al. The clustering of galaxies in the completed SDSS-III Baryon Oscillation Spectroscopic Survey: cosmological analysis of the DR12 galaxy sample. *Mon. Not. Roy. Astron. Soc.*, 470(3):2617–2652, 2017.

[90] D. M. Scolnic et al. The Complete Light-curve Sample of Spectroscopically Confirmed SNe Ia from Pan-STARRS1 and Cosmological Constraints from the Combined Pantheon Sample. *Astrophys. J.*, 859(2):101, 2018.

[91] Beth A. Reid et al. Cosmological Constraints from the Clustering of the Sloan Digital Sky Survey DR7 Luminous Red Galaxies. *Mon. Not. Roy. Astron. Soc.*, 404:60–85, 2010.

[92] F. Köhlinger et al. KiDS-450: The tomographic weak lensing power spectrum and constraints on cosmological parameters. *Mon. Not. Roy. Astron. Soc.*, 471(4):4412–4435, 2017.

[93] Benjamin Audren, Julien Lesgourgues, Karim Benabed, and Simon Prunet. Conservative Constraints on Early Cosmology: an illustration of the Monte Python cosmological parameter inference code. *JCAP*, 1302:001, 2013.

[94] Thejs Brinckmann and Julien Lesgourgues. MontePython 3: boosted MCMC sampler and other features. *Phys. Dark Univ.*, 24:100260, 2019.

[95] Antony Lewis. Efficient sampling of fast and slow cosmological parameters. *Phys. Rev.*, D87(10):103529, 2013.

[96] Sunny Vagnozzi, Elena Giusarma, Olga Mena, Katherine Freese, Martina Gerbino, Shirley Ho, and Massimiliano Lattanzi. Unveiling ν secrets with cosmological data: neutrino masses and mass hierarchy. *Phys. Rev.*, D96(12):123503, 2017.

[97] Tim Sprenger, Maria Archidiacono, Thejs Brinckmann, Sbastien Clesse, and Julien Lesgourgues. Cosmology in the era of Euclid and the Square Kilometre Array. *JCAP*, 1902:047, 2019.

[98] Ryuichi Takahashi, Masanori Sato, Takahiro Nishimichi, Atsushi Taruya, and Masamune Oguri. Revising the Halofit Model for the Nonlinear Matter Power Spectrum. *Astrophys. J.*, 761:152, 2012.

[99] Yacine Ali-Haimoud and Simeon Bird. An efficient implementation of massive neutrinos in non-linear structure formation simulations. *Mon. Not. Roy. Astron. Soc.*, 428:3375–3389, 2012.

[100] Antony Lewis. GetDist: a Python package for analysing Monte Carlo samples. 2019.

[101] Andrew Gelman and Donald B. Rubin. Inference from Iterative Simulation Using Multiple Sequences. *Statist. Sci.*, 7:457–472, 1992.

[102] Z. Chacko, Lawrence J. Hall, Takemichi Okui, and Steven J. Oliver. CMB signals of neutrino mass generation. *Phys. Rev.*, D70:085008, 2004.

[103] Graciela B. Gelmini, Shmuel Nussinov, and Marco Roncadelli. Bounds and Prospects for the Majoron Model of Left-handed Neutrino Masses. *Nucl. Phys.*, B209:157–173, 1982.

[104] Edward W. Kolb and Michael S. Turner. Supernova SN 1987a and the Secret Interactions of Neutrinos. *Phys. Rev.*, D36:2895, 1987.

[105] Kiwoon Choi and A. Santamaria. Majorons and Supernova Cooling. *Phys. Rev.*, D42:293–306, 1990.

[106] M. Kachelriess, R. Tomas, and J. W. F. Valle. Supernova bounds on Majoron emitting decays of light neutrinos. *Phys. Rev.*, D62:023004, 2000.

[107] Yasaman Farzan. Bounds on the coupling of the Majoron to light neutrinos from supernova cooling. *Phys. Rev.*, D67:073015, 2003.

[108] M. Doi, T. Kotani, and E. Takasugi. Double beta Decay and Majorana Neutrino. *Prog. Theor. Phys. Suppl.*, 83:1, 1985.

[109] M. Doi, T. Kotani, and E. Takasugi. The Neutrinoless Double Beta Decay With Majoron Emission. *Phys. Rev.*, D37:2575, 1988.

[110] Vernon D. Barger, Wai-Yee Keung, and S. Pakvasa. Majoron Emission by Neutrinos. *Phys. Rev.*, D25:907, 1982.

[111] A. P. Lessa and O. L. G. Peres. Revising limits on neutrino-Majoron couplings. *Phys. Rev.*, D75:094001, 2007.

[112] Giorgio Arcadi, Julian Heeck, Florian Heizmann, Susanne Mertens, Farinaldo S. Queiroz, Werner Rodejohann, Martin Slezák, and Kathrin Valerius. Tritium beta decay with additional emission of new light bosons. *JHEP*, 01:206, 2019.